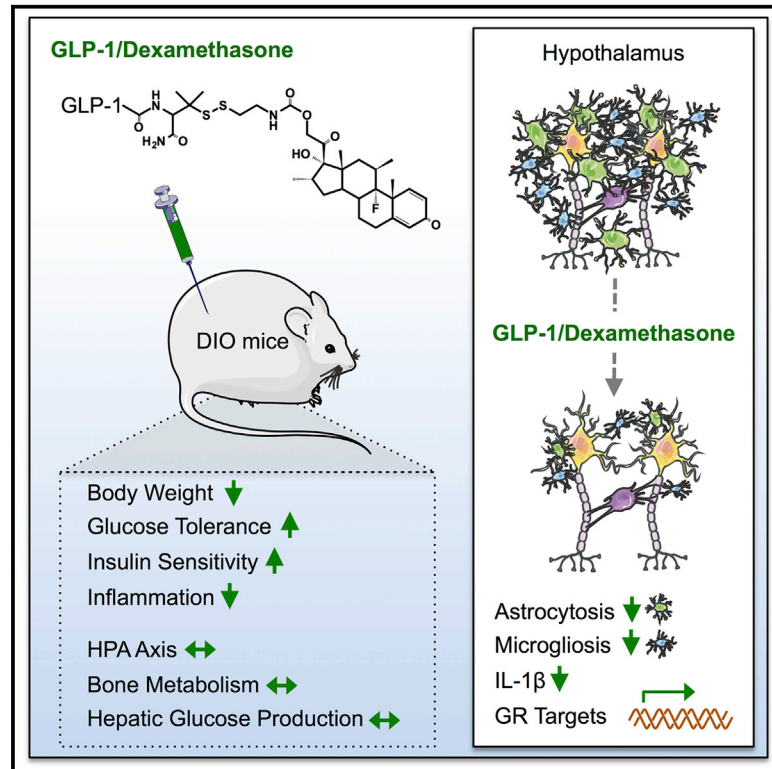


Cell Metabolism

Molecular Integration of Incretin and Glucocorticoid Action Reverses Immunometabolic Dysfunction and Obesity

Graphical Abstract



Authors

Carmelo Quarta,
 Christoffer Clemmensen,
 Zhimeng Zhu, ..., Richard D. DiMarchi,
 Brian Finan, Matthias H. Tschöp

Correspondence

brian.finan@helmholtz-muenchen.de
 (B.F.),
 matthias.tschoep@
 helmholtz-muenchen.de (M.H.T.)

In Brief

Quarta et al. develop a tissue-specific anti-inflammatory drug in which GLP-1 selectively delivers dexamethasone to GLP-1 receptor-expressing cells, bypassing many of the deleterious side effects of chronic dexamethasone treatment. The GLP-1/Dexa anti-inflammatory agent improves metabolism and lowers body weight up to 25% in obese mice through both central and peripheral effects.

Highlights

- A tissue-selective immunosuppressive agent reverses metabolic inflammation and obesity
- GLP-1/Dexa corrects hypothalamic and peripheral inflammatory-like processes in obese mice
- GLP-1/Dexa targets molecular pathways linking inflammation with cellular proteostasis
- GLP-1-directed delivery of Dexa actions circumvents adverse glucocorticoid effects

Molecular Integration of Incretin and Glucocorticoid Action Reverses Immunometabolic Dysfunction and Obesity

Carmelo Quarta,^{1,2,3,22} Christoffer Clemmensen,^{1,2,3,22} Zhimeng Zhu,⁴ Bin Yang,⁴ Sini S. Joseph,^{1,2,3} Dominik Lutter,^{1,2,3} Chun-Xia Yi,⁵ Elisabeth Graf,⁶ Cristina García-Cáceres,^{1,2,3} Beata Legutko,^{1,2,3} Katrin Fischer,^{1,2,3} Robert Brommage,⁷ Philippe Zizzari,^{8,9} Bernardo S. Franklin,^{10,11,12} Martin Krueger,¹³ Marco Koch,¹³ Sabine Vettorazzi,¹⁴ Pengyun Li,⁴ Susanna M. Hofmann,^{3,15,16} Mostafa Bakhti,^{3,15,17,18} Aimée Bastidas-Ponce,^{3,15,17} Heiko Lickert,^{3,15,17,18} Tim M. Strom,⁶ Valerie Gailus-Durner,⁷ Ingo Bechmann,¹³ Diego Perez-Tilve,¹⁹ Jan Tuckermann,¹⁴ Martin Hrabě de Angelis,^{3,7,20} Darleen Sandoval,²¹ Daniela Cota,^{8,9} Eicke Latz,^{10,11,12} Randy J. Seeley,²¹ Timo D. Müller,^{1,2,3} Richard D. DiMarchi,⁴ Brian Finan,^{1,2,3,23,*} and Matthias H. Tschöp^{1,2,3,*}

¹Institute for Diabetes and Obesity, Helmholtz Diabetes Center, Helmholtz Zentrum München, 85764 Neuherberg, Germany

²Division of Metabolic Diseases, Department of Medicine, Technische Universität München, 80333 Munich, Germany

³German Center for Diabetes Research (DZD), Helmholtz Zentrum München, Ingolstädter Landstraße, 85764 Neuherberg, Germany

⁴Department of Chemistry, Indiana University, Bloomington, IN 47405, USA

⁵Department of Endocrinology and Metabolism, Academic Medical Center, University of Amsterdam, 1105AZ Amsterdam, the Netherlands

⁶Institute of Human Genetics, Helmholtz Zentrum München, 85764 Neuherberg, Germany

⁷German Mouse Clinic, Institute of Experimental Genetics, Helmholtz Zentrum München, German Research Center for Environmental Health, 85764 Neuherberg, Germany

⁸INSERM

⁹University of Bordeaux

Neurocenter Magendie, Physiopathologie de la Plasticité Neuronale, U1215, F-33000 Bordeaux, France

¹⁰Institute of Innate Immunity, University Hospital, University of Bonn, 53127 Bonn, Germany

¹¹Department of Infectious Diseases and Immunology, University of Massachusetts Medical School, Worcester, MA 01605, USA

¹²German Center for Neurodegenerative Diseases, 53175 Bonn, Germany

¹³Institute for Anatomy, University of Leipzig, 04103 Leipzig, Germany

¹⁴Institute of Comparative Molecular Endocrinology, University of Ulm, 89081 Ulm, Germany

¹⁵Institute for Diabetes and Regeneration, Helmholtz Diabetes Center at Helmholtz Zentrum München, German Research Center for Environmental Health (GmbH), 85764 Neuherberg, Germany

¹⁶Medizinische Klinik und Poliklinik IV, Klinikum der LMU, 80336 Munich, Germany

¹⁷Institute of Stem Cell Research, Helmholtz Zentrum München, 85764 Neuherberg, Germany

¹⁸Technische Universität München, 81675 Munich, Germany

¹⁹Department of Internal Medicine, University of Cincinnati College of Medicine, Cincinnati, OH 45267, USA

²⁰Chair of Experimental Genetics, Center of Life and Food Sciences Weihenstephan, Technische Universität München, Munich, Germany

²¹Department of Surgery, University of Michigan, Ann Arbor, MI 48109-2800, USA

²²These authors contributed equally

²³Lead Contact

*Correspondence: brian.finan@helmholtz-muenchen.de (B.F.), matthias.tschoep@helmholtz-muenchen.de (M.H.T.)

<http://dx.doi.org/10.1016/j.cmet.2017.08.023>

SUMMARY

Chronic inflammation has been proposed to contribute to the pathogenesis of diet-induced obesity. However, scarce therapeutic options are available to treat obesity and the associated immunometabolic complications. Glucocorticoids are routinely employed for the management of inflammatory diseases, but their pleiotropic nature leads to detrimental metabolic side effects. We developed a glucagon-like peptide-1 (GLP-1)-dexamethasone co-agonist in which GLP-1 selectively delivers dexamethasone to GLP-1 receptor-expressing cells. GLP-1-dexamethasone lowers body weight up to 25% in obese mice by targeting the hypothalamic control of feeding and by increasing energy expendi-

ture. This strategy reverses hypothalamic and systemic inflammation while improving glucose tolerance and insulin sensitivity. The selective preference for GLP-1 receptor bypasses deleterious effects of dexamethasone on glucose handling, bone integrity, and hypothalamus-pituitary-adrenal axis activity. Thus, GLP-1-directed glucocorticoid pharmacology represents a safe and efficacious therapy option for diet-induced immunometabolic derangements and the resulting obesity.

INTRODUCTION

Inflammatory processes are elemental for cellular repair and serve as the vanguard defense mechanism against disease.

Regulation of these processes must be finely tuned in order to maintain homeostasis and avoid perturbations in cellular functions and disease. A surfeit of energy supply can disrupt metabolic homeostasis and exacerbate derangements in molecular mediators of immunity. This maladaptive state results in low-grade chronic inflammation that is suspected to be a pathogenic driver of the metabolic complications associated with diet-induced obesity (Hotamisligil, 2017).

Obesity-associated inflammation contributes to a plethora of metabolic dysfunctions in adipose tissue, liver, muscle, pancreas, and the gastrointestinal tract. This immunometabolic dysfunction is driven by invading immune cells, activation of dormant resident immune cells, and a perturbation of the reciprocal interactions between immune effectors and cells residing within a particular organ (Lumeng and Saltiel, 2011). Inflammatory processes associated with neuronal injury have also been observed in the central nervous system (CNS) of diet-induced obese (DIO) mice and obese humans. Hypercaloric environments trigger local immune responses in the mediobasal hypothalamus (Horvath et al., 2010; Milanski et al., 2009; Valdearcos et al., 2015), including the production of inflammatory cytokines that interfere with the regulation of energy metabolism and influence local hormonal sensitivity (Jais and Brüning, 2017; Kälin et al., 2015; Yi et al., 2017). These processes harmonize to adversely affect molecular programs that control homeostasis of intracellular proteins and organelles, culminating in neuronal stress (Cavadas et al., 2016; Ignacio-Souza et al., 2014; Ozcan et al., 2009, Yi et al., 2017).

Diet-induced obesity, leptin action, and insulin resistance can be improved in rodents by genetic disruption of inflammatory pathways in the hypothalamus (Douglass et al., 2017; Valdearcos et al., 2014, 2015; Zhang et al., 2008). Thus, translating these genetic strategies into pharmaceutical agents may be a relevant therapeutic strategy for treating the metabolic disease. However, pharmacological options targeting these central and peripheral pathogenic nodes of immunometabolism are not currently available or offer insufficient specificity. Although steroid-based anti-inflammatory drugs show translatable metabolic impact (Shoelson et al., 2006), unwanted off-target effects and scarce potency hinder their applicability. Glucocorticoid (GC)-based therapies are used to treat a multitude of inflammatory diseases, but their pleiotropic action can promote weight gain, osteoporosis, and gluco-metabolic complications (Schäcke et al., 2002).

We developed a series of combinatorial approaches that allow for precise delivery of nuclear hormones to distinct cellular subpopulations (Finan et al., 2012, 2016; Tschöp et al., 2016). Using glucagon-like peptide-1 (GLP-1) as a shuttle to transport estrogen to GLP-1 receptor (GLP-1R)-expressing cells, we showed selective delivery of estrogen to metabolically relevant organs in general, and hypothalamic cells specifically (Finan et al., 2012). Thus, we envisioned that coupling GLP-1 with an anti-inflammatory agent, specifically dexamethasone (Dexa), could selectively neutralize inflammatory-like processes in the hypothalamus, as well in other GLP-1R-positive tissues. Since GLP-1R is also expressed in peripherally active immune cells (Hadjijanni et al., 2010; Lynch et al., 2016; Marx et al., 2010), we hypothesized that such a strategy could be similarly effective for targeting the enhanced systemic inflammatory tone associated with obesity.

Here, we report that CNS and peripheral mechanisms are engaged by a GLP-1-based peptide that delivers Dexa, which improves multiple hypothalamic and systemic markers implicated in diet-induced inflammation, ultimately resulting in corrected metabolic abnormalities in obese mice. The selective preference for GLP-1R prevents hallmark liabilities associated with chronic Dexa therapy, including hyperglycemia, bone density deterioration, and alterations in the hypothalamus-pituitary-adrenal (HPA) axis, rendering this conjugated peptide an anti-inflammatory metabolic “smart drug.” Thus, molecular integration of incretin and GC pharmacology represents an initially counterintuitive, but ultimately promising, therapeutic strategy toward precision correction of pathogenic processes linking inflammation and obesity.

RESULTS AND DISCUSSION

Generation of GLP-1-Dexa Conjugates with Bioactive Linkers

We generated a series of GLP-1-Dexa conjugates with different linker chemistry that impart a range of molecular stabilities. Conjugation of Dexa did not influence the native potency of the parent GLP-1 analog. The measured EC_{50} of the GLP-1 analog at the human GLP-1R was 2 pM, whereas the EC_{50} of the three conjugates range from 1 to 7 pM. All conjugates feature a Dexa that was modified with a thiol-ethylamine group that is linked through a disulfide bond to a free thiol-containing amino acid at the C terminus of the GLP-1 backbone. These conjugates feature a bio-metabolizable linker that utilizes a bipartite, pro-drug release mechanism that results in native Dexa release in reducing conditions that resemble the intracellular environment (Figure S1A). Reduction of the disulfide bond liberates the thiol of the ethylamine Dexa adduct, and the resultant free thiol spontaneously cyclizes into the carbamate bond to the 21-position hydroxyl to release native Dexa. We finely tuned the structural integrity and biological stability of the disulfide bond through the selective use of cysteine homologs, homocysteine (Hey) and penicillamine (Pen), for coupling to the derivatized Dexa (Figure S1B). The three conjugates proved equally stable in neutral pH PBS and low glutathione concentration, a condition that mimics the extracellular environment (Figure S1C). In high glutathione concentration, a condition that mimics the intracellular environment, the hindered disulfide of the Pen conjugate was readily reduced, liberating Dexa but at a slower rate relative to the Cys conjugate (Figure S1D). However, the Pen-based conjugate was more stable in plasma relative to the other two conjugates (Figure S1E). The alkyl substitution adjacent to the disulfide that is present with Hey and Pen incrementally increased the stability of the disulfide bond relative to Cys. However, whether trace amounts of Dexa could leak from the peptide in circulation over time cannot be excluded.

Stable GLP-1-Dexa Conjugates Potently Lower Body Weight in DIO Mice

DIO mice were treated daily with subcutaneous injections of the different conjugates for 2 weeks (100 nmol/kg). The magnitude of the body weight (BW) loss directly correlated with the chemical stability of the linker. The Pen disulfide-based molecule (herein named GLP-1/Dexa) substantially decreased BW by

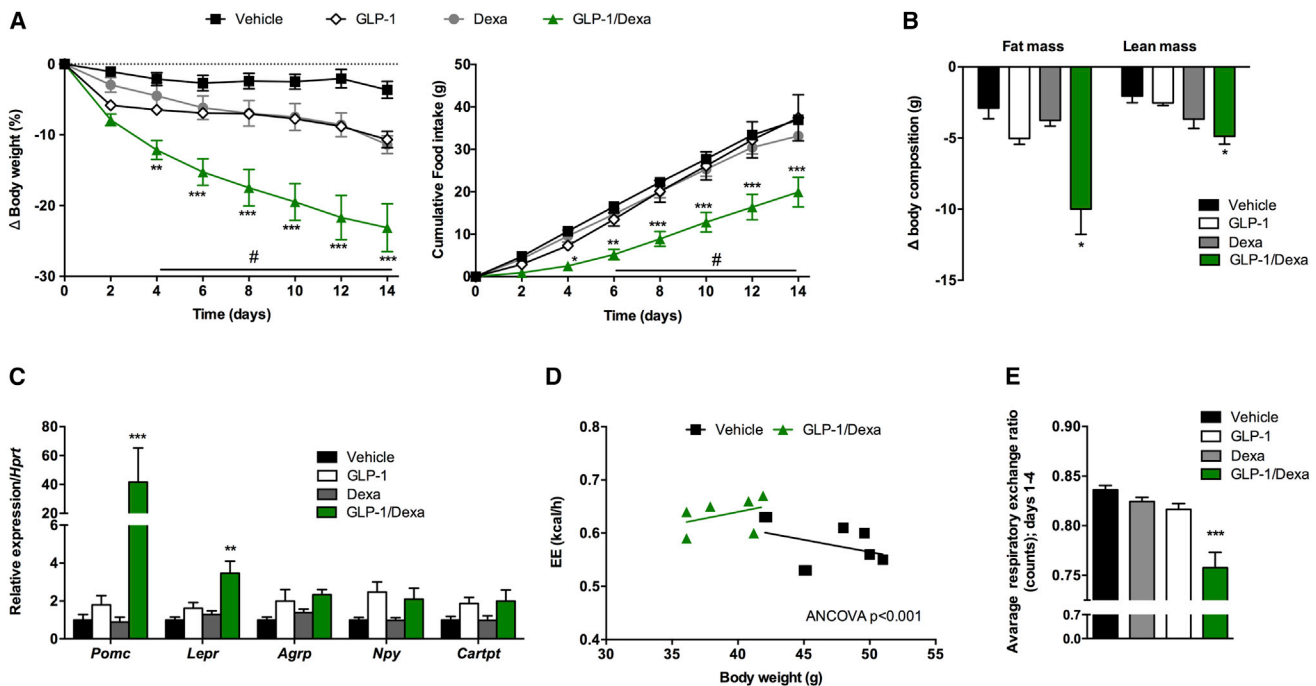


Figure 1. In Vivo Demonstration of the Metabolic Properties of GLP-1/Dexa in DIO Mice

For a Figure360 author presentation of Figure 1, see <http://dx.doi.org/10.1016/j.cmet.2017.08.023#mmc2>.

(A–C) Effects on BW, cumulative food intake (A), body composition change (days 0–14 of treatment) (B), and hypothalamic gene expression (C) in mice treated with GLP-1/Dexa or with equimolar doses of GLP-1 and Dexa for 14 days.

(D) Energy expenditure values (EE, kcal/hr) correlated to BW in mice treated with vehicle or with GLP-1/Dexa for 5 days. Lines show fitted regression.

(E) Average respiratory exchange ratio (RER) in animals treated with vehicle, GLP-1/Dexa, or equimolar doses of GLP-1 and Dexa for 5 days.

Data in (A)–(C) and (E) are expressed as mean \pm SEM. $n = 6$ –7 per group. * $p < 0.05$, ** $p < 0.01$, *** $p < 0.001$ by ANOVA comparing compound injection to vehicle unless otherwise noted. # $p < 0.01$ by ANOVA comparing GLP-1/Dexa versus GLP-1 and Dexa treatment.

25% from baseline and reduced cumulative food intake (Figure 1A). The Cys-disulfide and Hey-disulfide conjugates, which showed more degradation in plasma, caused less relative BW reduction (15%) and food intake suppression (Figure S2A). This indicates that biological stability influences the maximal metabolic efficacy of the conjugates, and the key to achieving weight-lowering efficacy resides in the meta-stable properties of the linker. The BW-reducing effects of the three GLP-1-Dexa conjugates were predominantly due to a loss in fat mass (Figures 1B and S2B). GLP-1/Dexa reduced BW, food intake, and adiposity to a greater level than equimolar, sub-threshold doses of GLP-1 or Dexa (Figures 1A and 1B), suggesting that the two singular components of the conjugates synergize to regulate metabolic balance.

In contrast to previous reports (Asensio et al., 2004), Dexa treatment did not induce hyperphagia or changes in the expression of hypothalamic neuropeptides (Figures 1A–1C). This discrepancy may be the result of the lower dose employed in our tests, which results in limited entry into the brain to modulate neuronal feeding circuits (Miller et al., 1992). Mice treated with GLP-1/Dexa exhibited significantly increased mRNA levels of the anorexigenic markers pro-opiomelanocortin (*Pomc*) and leptin receptor (*Lepr*) compared to vehicle, GLP-1, and Dexa treatments (Figure 1C), suggesting a potential role of the leptin-melanocortin axis in modulating the increased efficacy of GLP-1/Dexa.

The leptin-melanocortin axis is central to the metabolic efficacy of several anti-obesity drugs (Quarta et al., 2016). To evaluate if the feeding benefits of GLP-1/Dexa involve enhanced leptin responsiveness, we tested whether acute or chronic treatments influence the anorectic effects of an exogenous leptin bolus. Acute treatment with both GLP-1 and GLP-1/Dexa reduced feeding significantly and in a dose-dependent manner for the conjugate (Figure S2C). However, none of the treatments increased acute leptin responsiveness (Figure S2C). Seven-day treatment resulted in BW loss and suppression of feeding in mice that received compounds with GLP-1 activity, with the largest effect in mice that were treated with GLP-1/Dexa (Figure S2D). Close monitoring of feeding following the last injection revealed that mice previously treated with GLP-1 or the low dose of GLP-1/Dexa exhibited significant hyperphagia when compared to mice treated chronically with vehicle (Figure S2E). This suggests a waning efficacy at these doses and a simultaneous engagement of compensatory mechanisms promoting positive energy balance following the BW loss. Exogenous leptin prevented such hyperphagia in these two groups (Figures S2E and S2F), and was noticeably absent from mice that were calorically restricted to match the BW loss achieved by the high dose of GLP-1/Dexa (Figures S2G–S2I). This result points toward a reduction in endogenous leptin action in the absence of pharmacotherapy as one of those compensatory mechanisms aiming to restore positive energy balance in response to BW loss

(Figure S2E). In contrast, mice treated with the high dose of GLP-1/Dexa had a feeding pattern that was similar to that of vehicle-treated controls during the leptin challenge (Figures S2E and S2F). When compared to the lower dose, this suggests retention of sufficient pharmacological anorectic effect to prevent compensatory hyperphagia. Consequently, exogenous leptin did not result in further reduction of feeding (Figures S2E and S2F). Taken together, our findings demonstrate that increased anorectic efficacy of GLP-1/Dexa is not secondary to increased responsiveness to leptin.

To better characterize the metabolic properties of the conjugate, we measured energy expenditure using indirect calorimetry combined with analysis of covariance (ANCOVA) (Tschöp et al., 2011). GLP-1 and Dexa monotherapies did not alter energy expenditure relative to vehicle, whereas GLP-1/Dexa significantly increased oxygen consumption (Figures 1D and S3A). This effect is appreciably absent in peripherally administered GLP-1R mono-agonists (Harder et al., 2004), and further demonstrates dual pharmacology with multiple modes of action. The effect on energy expenditure was corroborated in a weight-clamping experiment, as calorie restriction exceeding the reduced food intake induced by GLP-1/Dexa was required to induce comparable BW loss (Figure S2G). GLP-1/Dexa also lowered the respiratory exchange ratio (RER) relative to vehicle and the monotherapies (Figure 1E), indicating enhanced lipid oxidation. Thus, stable chemical conjugation between GLP-1 and Dexa promotes favorable metabolic effects independently of enhanced leptin action, by empowering the anorectic actions of GLP-1 while introducing de novo effects on energy expenditure.

GLP-1/Dexa Improves Glucose Metabolism in DIO Mice

Classical GC action to increase hepatic glucose output directly opposes GLP-1 action. To determine if the attached Dexa negates the glycemic benefits of GLP-1, we investigated the gluco-metabolic effects of GLP-1/Dexa in various assays. Both GLP-1 and GLP-1/Dexa reduced fasting blood glucose in DIO mice following chronic treatment (Figure 2A). Dexa treatment increased fasted blood glucose levels (Figure 2A) and increased hepatic mRNA expression of the gluconeogenic markers glucose-6-phosphatase catalytic subunit (*G6pc*) and phosphoenol pyruvate carboxykinase 1 (*Pck1*) (Figure 2B), in agreement with its known diabetogenic effects (Schäcke et al., 2002). The induction of the gluconeogenic gene program was lower in livers of mice treated with GLP-1/Dexa compared to those treated with Dexa (Figure 2B). Since expression levels of GLP-1Rs are negligible in mouse hepatocytes (Bullock et al., 1996), these findings suggest that GLP-1-mediated delivery reduces the classical gluconeogenic action of Dexa by altering its natural biodistribution pattern to restrict access to the liver.

GLP-1 and GLP-1/Dexa comparably improved glucose tolerance in DIO mice relative to vehicle after 1 week (Figures S3B and S3C) and 2 weeks (Figure 2C) of treatment, while Dexa alone did not affect glucose clearance despite comparable BW loss relative to GLP-1 alone (Figure 1A). GLP-1/Dexa and GLP-1 equally increased glucose-stimulated insulin release relative to vehicle, whereas Dexa treatment did not influence insulin secretion (Figure 2D). This indicates that chemical conjugation of GLP-1 and Dexa does not alter the insulinotropic function of

the GLP-1 component of the conjugate. GLP-1/Dexa significantly improved insulin sensitivity relative to the other treatments (Figure 2E), most notably to GLP-1, which is likely a direct consequence of the enhanced weight-lowering efficacy of the conjugate. The HOMA-IR (homeostasis model assessment of insulin resistance) index was significantly reduced in animals treated with GLP-1 and GLP-1/Dexa, but not in mice treated with Dexa (Figure 2F).

Our data show that GLP-1/Dexa reverses glycemic complications associated with obesity in DIO mice and minimizes the negative impact of Dexa on hepatic gluconeogenesis. Further, the concomitant GC action does not impair the glycemic benefits elicited by GLP-1 action. Rather, the GLP-1 component counterbalances any potential diabetogenic liability of this dose of Dexa in a somewhat analogous fashion as with GLP-1/glucagon co-agonists (Day et al., 2009).

GLP-1/Dexa Affects Energy Balance via Dexa- and GLP-1-Specific Actions

To demonstrate the specificity of our approach, we analyzed genetic signatures specific for Dexa action in a GLP-1R-positive tissue, the hypothalamus, and GLP-1R-negative tissues, such as the liver and the thymus (Bullock et al., 1996), after chronic treatment of DIO mice. The conjugate, but not GLP-1 alone, increased the expression of the GR target genes GC-induced leucine zipper (*Tsc22d3*) and Kruppel-like factor 15 (*Klf15*) (Coutinho and Chapman, 2011; Patel et al., 2014) in the hypothalamus of DIO mice (Figure S4A). This demonstrates GLP-1R-mediated enrichment of GR transcriptional activity within the conjugate and confirms the presence of constituent Dexa activity. In those tissues that do not express GLP-1R, including both the liver and thymus, GLP-1/Dexa did not increase *Tsc22d3* and *Klf15* expression, whereas Dexa mono-therapy increased the mRNA levels of these GR-specific targets (Figure S4A). Accordingly, GLP-1/Dexa treatment significantly increased the expression of *Tsc22d3* and *Klf15* in primary hypothalamic neurons collected from wild-type (WT) mice, but not in neurons isolated from GLP-1R knockout animals (KO) (Figure S4B), demonstrating the selective preference for the conjugate to signal and deliver Dexa through GLP-1R.

To analyze whether GLP-1/Dexa possesses in vivo activity at GLP-1R, we used global GLP-1R KO mice. GLP-1/Dexa did not induce weight loss or reduce food intake in DIO mice with global deletion of GLP-1R (Scrocchi et al., 1996; here named global KO mice) (Figure 3A), indicating that the metabolic effects elicited by the conjugate are fully dependent on GLP-1R. These data suggest that GLP-1R-mediated delivery of Dexa is critically important to fully achieve Dexa-specific actions at the targeted site. Without the presence of GLP-1R on the cell surface, Dexa presumably cannot enter cells while covalently attached to the peptide. Thus, without these cellular gateways and the enhanced stability of GLP-1/Dexa in plasma, no residual Dexa effect is observed in GLP-1R negative tissues in vitro and in vivo.

While GLP-1Rs located in the CNS mediate the effects of GLP-1 agonists on BW control (Secher et al., 2014), peripheral mechanisms contribute to the favorable actions on glucose metabolism (Sisley et al., 2014). To analyze the contribution of central GLP-1Rs to the efficacy of GLP-1/Dexa, we used DIO mice with the selective ablation of GLP-1R in the entire CNS

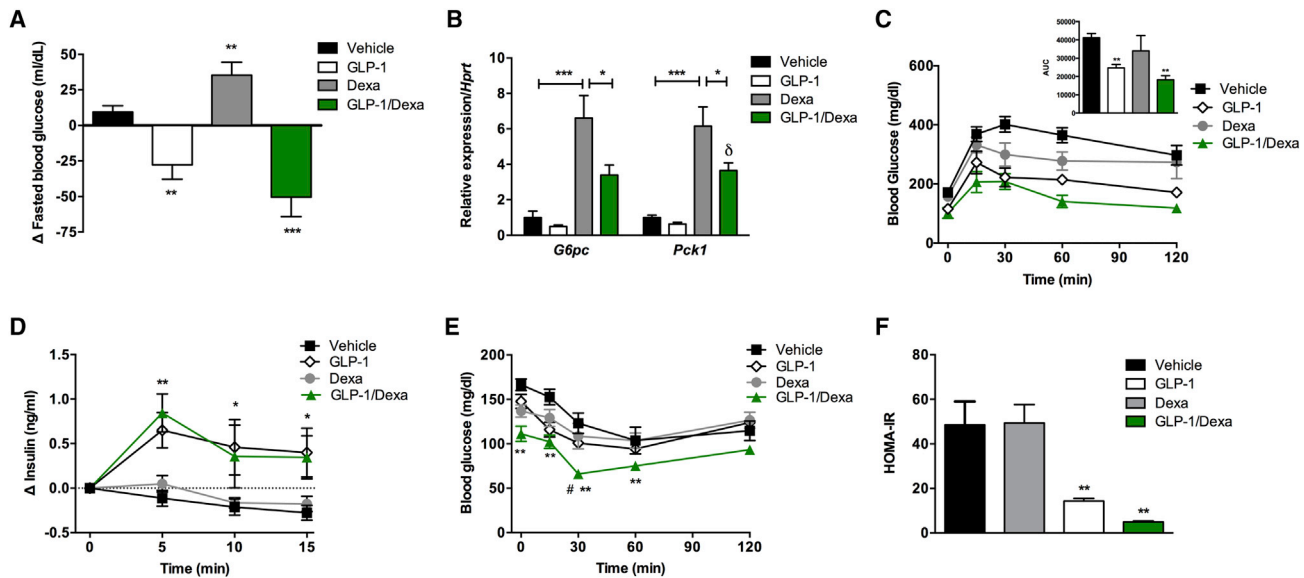


Figure 2. Gluco-Metabolic Effects of GLP-1/Dexa in DIO Mice

(A) Fasting (6 hr) blood glucose (Δ between days 0 and 13 of treatment) measured in DIO mice treated with vehicle, GLP-1/Dexa, or equimolar doses of GLP-1 and Dexa.
 (B) Gene expression analysis of livers from DIO animals treated with vehicle, GLP-1/Dexa, or equimolar doses of GLP-1 and Dexa for 14 days.
 (C) Glucose tolerance test performed in DIO animals treated with GLP-1/Dexa or with equimolar doses of GLP-1 and Dexa for 14 days.
 (D and E) Glucose-stimulated insulin secretion test (D) and insulin tolerance test (E) performed in DIO animals treated with GLP-1/Dexa or with equimolar doses of GLP-1 and Dexa for 16 days.
 (F) HOMA-IR (homeostasis model assessment of insulin resistance) calculated in DIO animals treated with GLP-1/Dexa or with equimolar doses of GLP-1 and Dexa for 16 days.

$n = 7-8$ per group. * $p < 0.05$, ** $p < 0.01$, *** $p < 0.001$ comparing vehicle to compound injections unless otherwise noted. $\delta p < 0.05$ comparing GLP-1/Dexa versus vehicle. In (D), * $p < 0.05$ and ** $p < 0.01$ comparing GLP-1 and GLP-1/Dexa versus vehicle and Dexa. In (E), ** $p < 0.01$ comparing GLP-1/Dexa versus vehicle, # $p < 0.05$ comparing GLP-1/Dexa versus GLP-1 and Dexa. Data were analyzed by ANOVA and are expressed as mean \pm SEM.

(Sisley et al., 2014; here named neuronal KO mice). The BW loss induced by GLP-1/Dexa was blunted in neuronal KO mice relative to WT controls, yet this was not a complete reversal as residual BW-lowering was still evident in neuronal KO mice (Figure 3B). The latter finding reveals that central and peripheral mechanisms contribute to the full BW-lowering efficacy of the conjugate. This also demonstrates that GLP-1 not only serves as a vehicle for delivery of Dexa to the brain, but it also actively contributes to pharmacological virtues of the conjugate. GLP-1/Dexa was equally effective at improving glucose tolerance in neuronal KO and WT animals (Figure 3B), suggesting that central GLP-1Rs are not involved in mediating the glycemic benefits of GLP-1/Dexa, which is aligned with observations of GLP-1R monoagonists (Sisley et al., 2014). To further analyze the involvement of the CNS, we tested whether intracerebroventricular administration of GLP-1/Dexa promoted metabolic changes. This approach significantly lowered food intake and BW in DIO mice (Figure S4C), but did not affect fasting glycemia (Figure S4D), confirming that CNS-based mechanisms are responsible for the BW-lowering effects of the conjugate, but they are dispensable for the gluco-metabolic actions.

The endocrine pancreas mediates the majority of glycemic benefits among GLP-1-based pharmacological actions (Cho et al., 2014; Smith et al., 2014). To analyze the specific contribution of islet GLP-1Rs, we used DIO mice with the selective ablation of GLP-1Rs in β cells (Smith et al., 2014; here named

β cell-KO) and control littermates. The acute glucose tolerance benefits of GLP-1/Dexa were completely abolished in β cell-KO mice relative to controls (Figure 3C). Conversely, following chronic treatment with GLP-1/Dexa, both BW and glycemic benefits were similar between β cell-KO mice and WT controls (Figure 3D). Thus, whereas β cell GLP-1Rs are necessary for the acute effects of GLP-1/Dexa on glucose tolerance, these receptors are dispensable when it comes to the benefits on BW and glucose tolerance following chronic treatment with GLP-1/Dexa. This highlights a lack of information within the scientific community on how extra-pancreatic tissues harboring GLP-1Rs mediate the gluco-metabolic effects of GLP-1-based pharmacotherapies, and also an under appreciation of the contribution of the weight-lowering action to the glycemic actions. We did not observe major histomorphological changes in islet architecture and composition after chronic GLP-1/Dexa treatment (Figure S4E). GLP-1/Dexa significantly increased the number of insulin positive cells, in agreement with its insulinotropic activity, but did not induce changes in the percentage of glucagon and somatostatin positive cells (Figure S4F).

Together, these data show that GLP-1/Dexa affects energy metabolism via both Dexa and GLP-1-specific actions, involving CNS and peripherally mediated mechanisms. GLP-1R expressing cells beyond the CNS and the β cells appear critical for the long-term glycemic benefits of the GLP-1/Dexa, and these same cells may be contributing to the energy metabolism

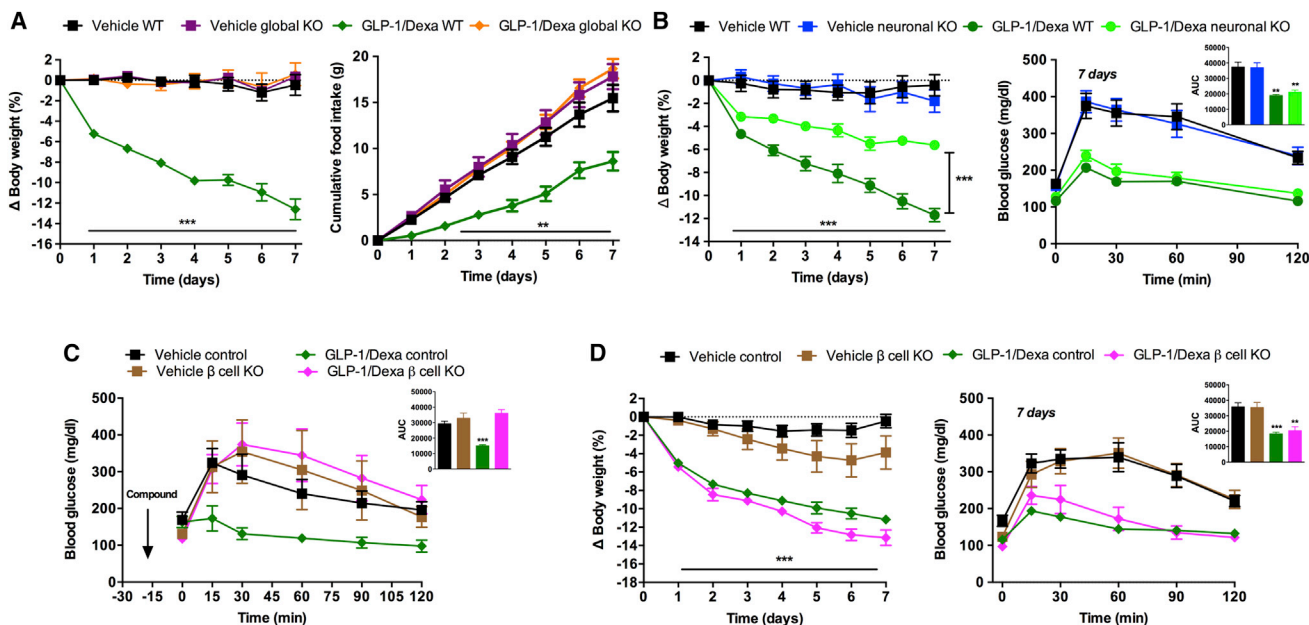


Figure 3. GLP-1/Dexa-Specific Actions

(A) Effects on BW and cumulative food intake in DIO WT mice and DIO mice with global ablation of GLP-1R (global KO) treated with GLP-1/Dexa or vehicle for 7 days.

(B) Effects on BW and glucose tolerance in DIO WT mice and DIO mice with CNS-specific ablation of GLP-1R (neuronal KO) treated with GLP-1/Dexa for 7 days.

(C) Effects on glucose tolerance in DIO mice with β cell-specific ablation of GLP-1R (β cell KO) and control littermates acutely treated by intraperitoneal administration of vehicle or GLP-1/Dexa (10 nmol/kg) 15 min prior to the test.

(D) Effects on BW and glucose tolerance in DIO mice with β cell-specific ablation of GLP-1R (β cell KO) and control littermates treated with GLP-1/Dexa or vehicle for 7 days.

n = 7–10 per group. **p < 0.01, ***p < 0.001 comparing GLP-1/Dexa to vehicle treatment, independently from genotype, unless otherwise noted. In (A), ***p < 0.001, **p < 0.01 comparing GLP-1/Dexa versus all the other treatments. AUC, area under the curve. Data were analyzed by ANOVA and are expressed as mean \pm SEM.

benefits. Accordingly, GLP-1Rs residing outside the islets may co-modulate GLP-1/Dexa mediated actions on glucose homeostasis by a yet-to-be determined paracrine signaling mechanism (Smith et al., 2014). While this mechanism may not be relevant for GLP-1 monoagonism, identification of the exact GLP-1R-expressing cell populations mediating additional metabolic effects engaged by multi-agonists, GLP-1/Dexa included, could give rise to other promising unimolecular combinatorial therapeutics.

No Metabolic Impact of GLP-1/Dexa in Mice Fed with Chow Diet

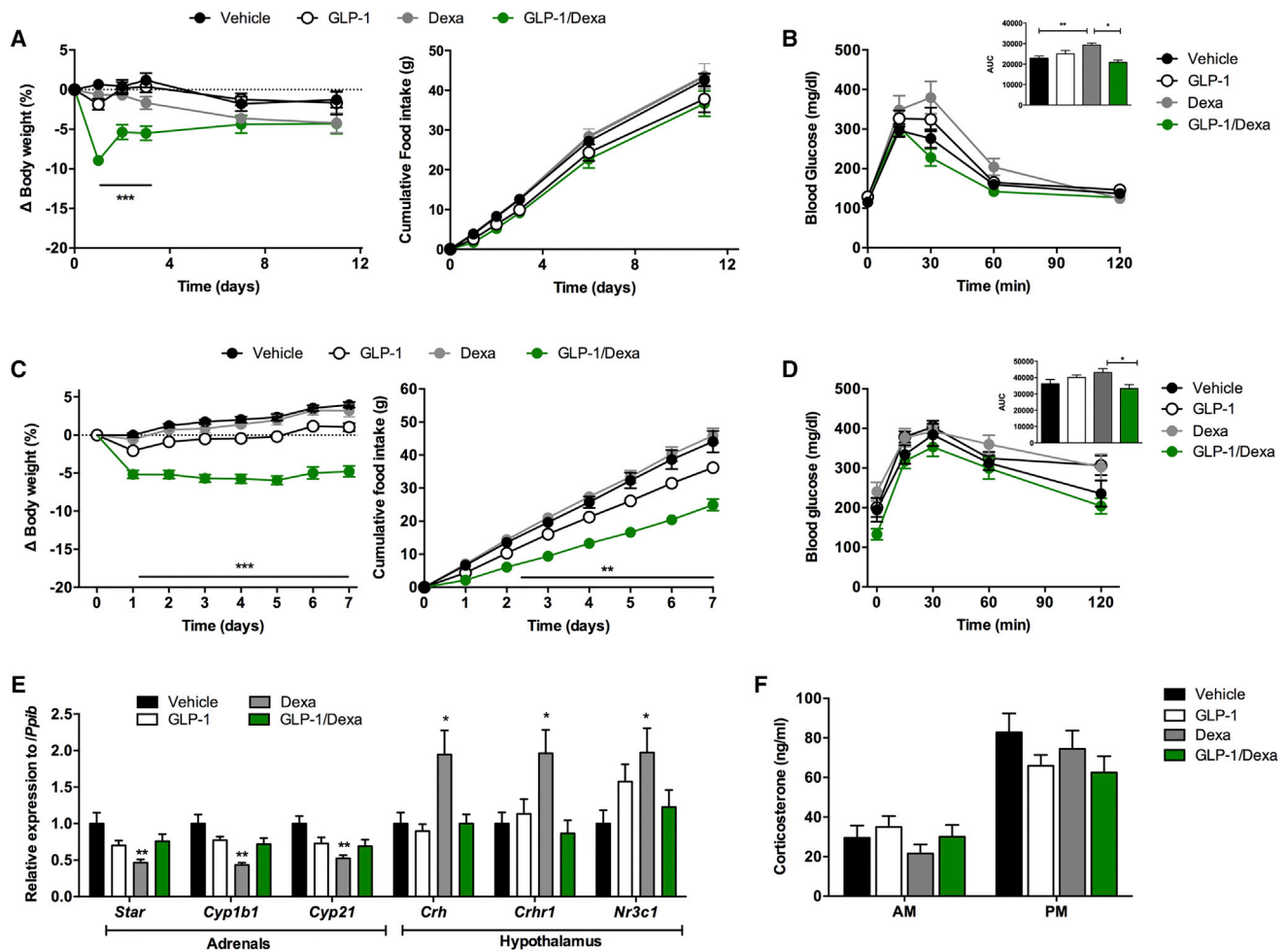
To investigate whether the metabolic effects observed are specific for diet-induced obesity, we tested the effects of GLP-1/Dexa in lean control mice and in genetically obese *ob/ob* mice fed a chow diet (CD). Despite inducing a transitory BW loss and food intake reduction in lean CD mice (Figures 4A and S5A), chronic treatment with GLP-1/Dexa did not significantly impact these endpoints (Figure 4A). The expression of hypothalamic neuropeptides involved in the control of feeding was not altered by GLP-1/Dexa in CD mice (Figure S5B), which is in direct contrast to what was observed in DIO mice (Figure 1C). Comparable *Glp1r* mRNA levels were quantified in the hypothalamus of lean CD mice relative to DIO animals (Figure S5C), suggesting that the lack of pharmacological efficacy in these animals could not be explained by reduced relative receptor abundance in this

region. Whereas an equimolar dose of Dexa impaired glucose tolerance, GLP-1/Dexa and GLP-1 treatments at these doses did not affect glucose clearance in lean CD mice (Figure 4B), a finding in agreement with the lack of Dexa-like diabetogenic effects following treatment of DIO mice with GLP-1/Dexa (Figure 2).

GLP-1/Dexa reduced BW and food intake in CD-fed obese *ob/ob* mice to a greater magnitude than the mono-therapies (Figure 4C), although the efficacy was somewhat reduced in comparison to that observed in the DIO mice (Figure 1A). Also, in contrast to the improved glucose tolerance observed in DIO mice, the conjugate did not improve glucose control in *ob/ob* mice (Figure 4D). Thus, different from the prominent anti-obesity and anti-diabetic effects achieved in DIO animals (Figure 1), blunted metabolic effects were observed in lean and genetically obese mice on a CD (Figure 4), suggesting that GLP-1/Dexa primarily targets pathological processes driven by diet-induced obesity.

GLP-1/Dexa Does Not Induce Adverse Effects Indicative of Systemic GC Action

Prolonged GC treatment can result in alterations in bone metabolism and the feedback suppression of the HPA axis (Schäcke et al., 2002). We tested whether the conjugate impacts HPA axis regulation and bone integrity. Dexa mono-therapy suppressed



the expression of several genes involved in the regulation of steroid metabolism in adrenal glands and increased the expression of markers of HPA activity in the hypothalamus (Figure 4E). The disparate direction of this gene expression profile is likely due to adrenal sensing of peripheral GC action resulting in compensatory central feedback on the HPA axis as opposed to a direct hypothalamic action since the dose of Dexa used is expected to have negligible brain penetration (Miller et al., 1992). The lack of modulation of Dexa-specific targets in the hypothalamus (Figure S4A) reaffirms that the doses of peripheral Dexa employed here have limited brain penetration. GLP-1/Dexa did not impact any of these transcriptional markers (Figure 4E), which indicates that the GLP-1 carrier is not delivering Dexa to peripheral or hypothalamic cell populations that govern HPA axis regulation.

Consistent with gene expression profiling, GLP-1/Dexa did not affect plasma levels of corticosterone (Figure 4F). However, circulating corticosterone levels were also not affected by equimolar Dexa treatment (Figure 4F). This lack of physiological manifestation following Dexa therapy again likely reflects the limited access of Dexa to the brain at these relatively low doses (Miller et al., 1992), which manifests into minimal impact on HPA axis regulation. Accordingly, higher doses of Dexa profoundly suppressed the expression of steroidogenic genes in adrenals (Figure S5D) and clearly lowered corticosterone levels (Figure S5E) relative to vehicle treatment.

None of the treatments induced changes in whole-body and spine bone mineral density (Table 1). GLP-1/Dexa also did not affect plasma markers of bone metabolism: CTX-1

Table 1. Analysis of Bone Mineral Density by DEXA Scan and Plasma Markers of Bone Metabolism

Treatment	Body BMD (mg/cm ²)	Spine BMD (mg/cm ²)	CTX-1 (ng/mL)	PINP (ng/mL)
Vehicle	71.4 ± 2.7	58.9 ± 4.3	12.0 ± 2.5	45.7 ± 15.2
Dexamethasone	73.0 ± 2.8	60.6 ± 3.1	13.0 ± 3.3	34.4 ± 16.7
GLP-1	71.6 ± 2.3	59.9 ± 3.1	12.3 ± 1.8	39.4 ± 11.6
GLP-1/Dexa	71.9 ± 1.8	60.6 ± 1.2	9.7 ± 0.8	33.3 ± 7.7

Data are means ± SD. n = 8 mice per group. BMD, bone mineral density; CTX-1, carboxy-terminal collagen crosslinks; PINP, N-terminal propeptide of type I collagen.

(carboxy-terminal collagen crosslinks) and PINP (N-terminal propeptide of type I collagen) (Table 1). Collectively, these findings reveal that GLP-1/Dexa does not induce negative effects on bone integrity and HPA axis activity within these experimental settings. The lack of adverse side effects reflects the negligible GLP-1R expression in bone and adrenal glands (Bullock et al., 1996), and in the absence of GLP-1R in these tissues, exposure to Dexa is minimized with GLP-1-mediated targeting, which exploits the many benefits associated with GC action.

GLP-1/Dexa Promotes Intracellular Organelle Homeostasis and Reverses Hypothalamic Inflammation

To further elucidate the *in vivo* signaling properties of GLP-1/Dexa, we performed unbiased transcriptional profiling (mRNA-seq) of hypothalami from treated DIO mice. A group of calorie-restricted (CR) mice with BW matched to that of GLP-1/Dexa-treated mice (Figure S6A) was included in order to dissect whether the molecular signatures governed by the conjugate are independent from the induced weight loss. We demonstrate a considerable overlap in gene program alterations induced by GLP-1/Dexa relative to Dexa or GLP-1 mono-therapies (Figure 5A), suggesting that both GLP-1-sensitive and Dexa-sensitive signaling events are elicited in the hypothalamus by the conjugate. In addition, a unique set of 126 genes was altered by GLP-1/Dexa (Figure 5A), revealing that the conjugate possesses unique signaling properties *in vivo*. However, this unique gene set could also be the consequence of signaling synergism that empowers the GLP-1- and Dexa-sensitive pathways to amplify their distinctive gene responses.

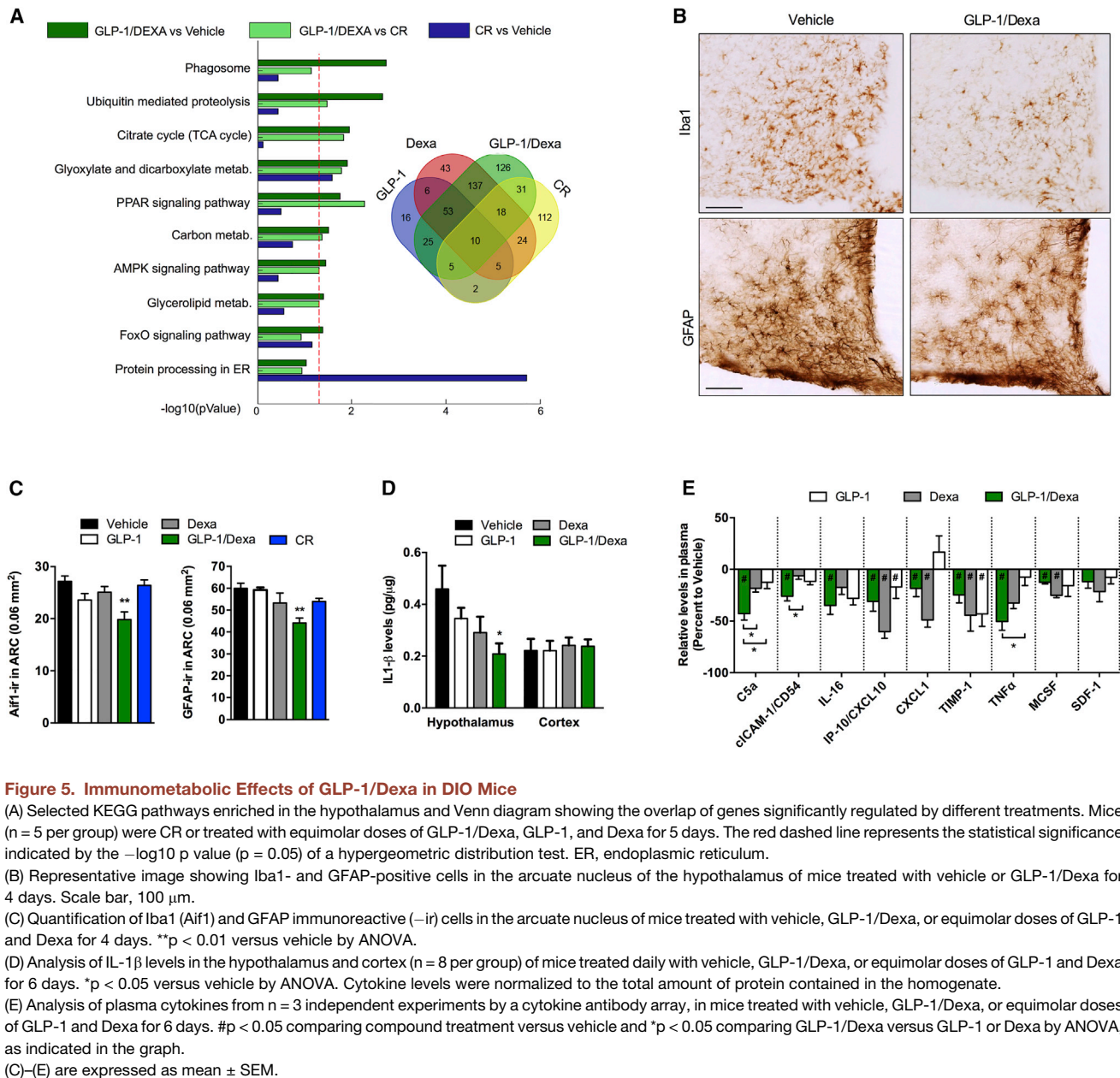
We identified several functional patterns differentially regulated by GLP-1/Dexa relative to vehicle, including pathways previously connected to diet-induced hypothalamic inflammation such as autophagy, ubiquitin-mediated proteolysis, and endoplasmic reticulum (ER) processing (Ignacio-Souza et al., 2014; Ozcan et al., 2009; Valdearcos et al., 2015) (−log₁₀ p value > 1.3; Figure 5A). Pathways relevant for fuel sensing and intercellular adaptation to energy availability (FOXO1, TCA cycle, and PPAR signaling pathways) were also enriched by GLP-1/Dexa (Figure 5A). Apart from the ER processing pathway, these genetic programs enriched by the conjugate were not altered in CR mice, indicating that these pathways are not simply induced by changes in BW and food intake (Figure 5A). Thus, GLP-1/Dexa directly regulates hypothalamic gene networks responsible for intracellular energy homeostasis, organelle rearrangements, and autophagy. Accordingly, GLP-1/Dexa lowered the

number of lipofuscin-positive granules in hypothalamic POMC-expressing neurons (Figures S6B and S6C). The accumulation of these intracellular products is indicative of dysfunctional lysosome activity and altered cellular integrity (Kurz et al., 2008) that correlates with the reduced POMC expression associated with hypercaloric diets and hypothalamic injury (Thaler et al., 2012). This indicates that part of the mechanism for GLP-1/Dexa is to correct diet-induced alterations in neuronal organelle homeostasis and POMC expression restoration. Likely, the resetting of deranged cellular physiology contributes to the increased expression of *Pomc* following GLP-1/Dexa treatment (Figure 1C) as opposed to a direct effect of the Dexa component since GC action has been shown to downregulate hypothalamic POMC levels (Jeanneteau et al., 2012).

We explored the molecular actions of GLP-1/Dexa in the context of lessening hypothalamic inflammation. The unbalanced regulation of protein and organelle homeostasis in hypothalamic neurons (“proteostasis”) is often accompanied by the activation of inflammatory responses (Cavadas et al., 2016). One such process is the recruitment and activation of hypothalamic glial cells, which is an early adaptive response to nutrient excess (Thaler et al., 2012). If continually hyperactivated, these glial cells release pro-inflammatory cytokines that may exacerbate neuronal injury and cellular stress provoked by diet-induced obesity (Kälin et al., 2015; Thaler et al., 2012). The accumulation of activated astrocytes results in an increase in the surrogate astrocyte marker glial fibrillary acidic protein (GFAP), and hyperactivated microglia cells are paralleled by an increase in the microglia marker ionized calcium binding adaptor molecule 1 (*Aif1*, also known as *Iba1*). GLP-1/Dexa treatment reduced the immunoreactivity (Figures 5B and 5C) and transcript levels (Figure S6E) of these glia markers in the hypothalamus, whereas the mono-therapies and caloric restriction had no effect (Figure 5C).

The NLRP3 inflammasome is a multimeric protein complex that activates the pro-inflammatory cytokine interleukin-1 beta (IL-1β), and this pathway has been implicated in diet-induced peripheral insulin resistance (Vandanmagsar et al., 2011) and neurological disorders (Heneka et al., 2013). GLP-1/Dexa reduced hypothalamic levels of active IL-1β by 3-fold relative to vehicle, while cerebral cortex levels of IL-1β were unaltered (Figure 5D). This area of the brain expresses negligible GLP-1R levels relative to the hypothalamus (Cork et al., 2015), suggesting that the conjugate selectively downregulates the pro-inflammatory profile of tissues with a sufficient amount of GLP-1R. Levels of interleukin 6 (IL-6) were unchanged following GLP-1/Dexa treatment (Figure S6D), and tumor necrosis factor alpha (TNFα) was undetectable in these preparations.

Collectively, these data reveal that GLP-1/Dexa selectively reverses dietary-induced inflammatory processes in a GLP-1R-dependent manner. Such immunomodulatory actions are independent from the effects of the conjugate to lower BW and food intake, and it is likely driven by the concerted action of the Dexa and GLP-1 components to reset the dysregulated molecular programs governing intracellular organelle homeostasis. Thus, GLP-1/Dexa treatment may offer therapeutic potential to correct diet-induced alterations in functional integrity of hypothalamic neurons by targeting molecular pathways connecting diet-induced inflammation with cellular proteostasis.



GLP-1/Dexa Ameliorates Diet-Induced Systemic Inflammation

GLP-1Rs are functionally active in peripheral T and B lymphocytes (Hadjiyanni et al., 2010; Marx et al., 2010). Thus, GLP-1-mediated delivery of Dexa to peripheral immune cells might promote systemic immunometabolic effects. To assess this potential action, we measured plasma levels of inflammatory markers pathologically altered during obesity. Treatment of DIO mice with GLP-1/Dexa induced a prominent reduction in chemotactic peptides linked to high-fat-diet-induced vascular inflammation, such as the complement component C5a (Osaka et al., 2016) and soluble intercellular adhesion molecule-1 sICAM1 (Shai et al., 2006). The conjugate reduced plasma levels of cytokines involved in T cell recruitment, insulin resistance, and

diabetes, including the chemokine (C-X-C motif) ligands CXCL1, CXCL10, and interleukin 16 (Dufour et al., 2002; Kim et al., 2014a; Meagher et al., 2010) (Figures 5E and S7F). Moreover, GLP-1/Dexa lowered inflammatory markers upregulated in obesity including the tissue inhibitor of matrix metalloproteinase 1 (TIMP-1) (Kralisch et al., 2007; Meissburger et al., 2011) and the macrophage colony-stimulating factor (MCSF) (Weisberg et al., 2003) (Figure 5E). A similar impact was observed for the pro-inflammatory cytokines TNF- α and IL-1- α (Figures 5E and S6F). GLP-1 or Dexa treatment alone induced comparable systemic anti-inflammatory actions, albeit the conjugate lowered C5a, sICAM1, and TNF α to a greater extent (Figure 5E). Relative to mice treated with GLP-1/Dexa, CR mice did not display a similar reduction in the plasma levels of most of these markers

(Figure S6F), indicating that these systemic effects are a direct result of the pharmacology and not indirectly triggered as a consequence of weight loss. Reduced mRNA levels of markers indicative of macrophage infiltration were quantified in the visceral adipose tissue of animals treated with GLP-1-Dexa, GLP-1, and Dexa mono-therapy for 7 days (Figure S6G). Whereas this sub-chronic treatment did not change the number of crown-like structures (CLSs) (data not shown), a prolonged treatment (16 days) effectively reduced the amount of CLSs in the visceral fat (Figures S6H and S6I), suggesting that the long-term systemic anti-inflammatory actions translate into reduced local inflammation in adipose tissues.

We conclude that GLP-1/Dexa possesses central and peripheral anti-inflammatory actions, which are not merely a consequence of BW loss. Rather, they likely originate from the concerted immunosuppressive effects induced by both the GLP-1 and the Dexa components in GLP-1R-expressing immunometabolic cells (Hadjiyanni et al., 2010; Lynch et al., 2016; Marx et al., 2010). Such reduced systemic inflammation is aligned with the pharmacological actions of GLP-1 to positively impact insulin sensitivity, glucose metabolism, and adiposity.

Perspective

We provide a proof-of-concept use of a cell-selective immunosuppressive agent for the safe treatment of metabolic inflammation and obesity. Our data show that GLP-1-directed targeting of GC action offers the therapeutic opportunity to alleviate pathogenic nodes connecting diet-induced inflammation with obesity. GLP-1 provides a feasible means to deliver Dexa to cells in the CNS and periphery, expanding the metabolic action profile of GLP-1R agonism by harnessing a specific subset of Dexa effects that provide additional immunometabolic modulation. Some of these benefits induced by Dexa alone can only be achieved by much higher doses, which undoubtedly cause unwanted side effects. The precision targeting afforded by the GLP-1 transporter alters the biodistribution of Dexa by restricting action to only those tissues housing GLP-1R, which produces less of an adverse effect on bone, liver, and adrenals than otherwise observed with untargeted Dexa, while also capitalizing on the dual pharmacodynamics afforded by this hormonal pairing.

GLP-1/Dexa targets both hypothalamic and peripheral immunometabolic mechanisms that govern the pleiotropic metabolic benefits of the conjugate. The complexity and redundancy of chronic metabolic inflammation necessitates the use of multi-acting, combinatorial therapies that engage multiple meta-inflammatory components (Hotamisligil, 2017). The incretin-GC fusions presented herein represent a promising therapy fitting the criteria. Future studies are required to dissect the exact identity of the GLP-1R-expressing cells that coordinate the glycemic, inflammatory, and weight-lowering properties of GLP-1/Dexa. Such studies could address recent work suggesting that GLP-1R-expressing peripheral immune cells are required for maximal weight loss induced by GLP-1R agonists (Lynch et al., 2016), as well as the contribution of non-neuronal glial cells in the hypothalamus that modulate energy balance (Douglass et al., 2017) and respond to hormonal cues (García-Cáceres et al., 2016; Kim et al., 2014b). Moreover, a comprehensive screening of the cellular and molecular underpinnings of GLP-1/Dexa actions at target sites will potentially elucidate the underlying mecha-

nisms that drive weight loss, which are likely a constellation of factors as opposed to a singular molecular pathway.

Central for translational value, the GLP-1R selectivity of our pharmacological approach has the advantage of safely exploiting the immunosuppressive properties of Dexa while minimizing negative metabolic effects (hyperglycemia, bone deterioration, disrupted HPA axis regulation, and visceral fat accumulation) typically observed with GC-based chronic administration. Thus, our study might ignite a paradigm shift toward the development of targeted anti-inflammatory steroids. However, uncertainties regarding the chronic use of Dexa remain, as insulin resistance is observed in patients on chronic Dexa therapy and in individuals with GC overexposure like in Cushing's disease (Geer et al., 2014). While we monitored the effects of the conjugate in rodents over a 2-week window without observing a worsening in insulin sensitivity, prolonged treatments should be assessed before translating our findings into clinically applicable therapeutics. In context, the same limitations confronting the use of classical immunological modulators are apparent with our conjugate. Notably, the degree of immunosuppressive effects is a delicate balance and must be considered for at least three reasons: (1) an active immune response is vital for maintaining proper metabolic homeostasis of parenchymal cells; (2) complete suppression of the immune response may compromise molecular and cellular repair, thus paradoxically propagating inflammation-induced cellular injury; and (3) immunosuppressive effects may compromise the body's ability to defend from invading foreign antigens.

Chemical refinement may also be required before proceeding to clinical studies. Such refinements could include optimizing the *in vivo* time of action or fine-tuning the meta-stable properties of the linker. Introducing additional complementary pharmacologies is hypothetically possible, including within the targeting peptide by integrating amino acid mutations that permit action at other related receptors. However, as mixed agonism is built into the targeting peptide, a broadened biodistribution is inherently expected and could mitigate the improved therapeutic index achieved by a more precise targeting approach of GLP-1R monoagonism. Heterologously decorating the peptide with nuclear hormones of a diverse nature is also possible, but mechanisms and potency need to be compatible. Naturally, before these agents can reach clinical study, more pre-clinical trials are required to determine whether our approach will be suitable for broad patient populations or for subpopulations of patients with inflammatory and metabolic co-morbidities. Controversy still exists whether inflammation is directly involved in the pathogenesis of human obesity or whether this is simply more pronounced in rodents. Although biologics aimed to block interleukin and cytokine actions have shown profound clinical benefits in chronic inflammatory diseases such as rheumatoid arthritis, psoriasis, and Crohn's disease, modest promise has been shown for these agents to improve metabolic control. This is largely because of disparaging variation in the results (Donath, 2014), but also because the immunosuppressive side effects are likely dose limiting (Donath et al., 2013). Precisely for this reason, we remain optimistic that our cell-specific anti-inflammatory approach has metabolic medicinal potential and also offers prospects as a platform that can be extended to other inflammatory conditions such as inflammatory bowel diseases and

rheumatoid arthritis through the judicious selection of the homing protein and anti-inflammatory payload.

STAR★METHODS

Detailed methods are provided in the online version of this paper and include the following:

- [KEY RESOURCES TABLE](#)
- [CONTACT FOR REAGENT AND RESOURCE SHARING](#)
- [EXPERIMENTAL MODEL AND SUBJECT DETAILS](#)
 - Mice
- [METHOD DETAILS](#)
 - Peptide Synthesis and Validation
 - Body Composition Measurements
 - Dual-Energy X-Ray Absorptiometry (DEXA)
 - Glucose Metabolism Assessments
 - Leptin Challenge
 - Indirect Calorimetry
 - Intracerebroventricular (i.c.v.) Studies
 - Gene Expression Analysis by qPCR
 - Corticosterone Measurement
 - Markers of Bone Metabolism
 - Immunohistochemistry
 - Adipose Tissue Histology
 - Electron Microscopy
 - Hypothalamic Cytokine Measurement
 - Plasma Cytokine Measurement
 - Culture of Hypothalamic Primary Neurons
 - RNA Sequencing
- [QUANTIFICATION AND STATISTICAL ANALYSIS](#)
- [DATA AND SOFTWARE AVAILABILITY](#)

SUPPLEMENTAL INFORMATION

Supplemental Information includes six figures and one table and can be found with this article online at <http://dx.doi.org/10.1016/j.cmet.2017.08.023>.

AUTHOR CONTRIBUTIONS

C.Q. and C.C. researched and interpreted the data and wrote the manuscript. R.D.D. conceptualized the project and interpreted all data. B.F. and M.H.T. conceptualized the project, interpreted the data, and co-wrote the manuscript with C.Q. and C.C. All the other authors researched the data and edited the manuscript.

CONFLICTS OF INTEREST

E.L. is co-founder of and consultant to IFM Therapeutics. M.H.T. serves as a consultant for Bionorica, Novo Nordisk Pharmaceuticals, and ERX Pharmaceuticals and received research support from Bionorica and Sanofi S.A. R.J.S. receives research support from Ethicon Endo-Surgery/Johnson & Johnson, Novo Nordisk, Janssen/Johnson & Johnson, Medimmune, Boehringer-Ingelheim, and Sanofi, where he also serves as a consultant. R.J.S. serves as a consultant for Novartis, Orexigen, Takeda, Daiichi Sankyo, Paul Hastings Law Firm, and Zafgen. B.F., B.Y., P.L. and R.D.D. are current employees of Novo Nordisk. The research in this publication was not supported financially by Novo Nordisk. R.D.D. is a founder of Calibrum Biotech, LLC.

ACKNOWLEDGMENTS

We thank Heidi Hofmann, Jack Magrisso, Stace Kernodle, Laura Seherer, Luisa Müller, Daniela Heine, Sigrid Jall, Joyce Sorrell, and Cynthia Striese for assis-

tance with in vivo experiments. We thank Sandy Lösecke for technical assistance in RNA library preparation and Thomas Schwarzmayr for assistance with bioinformatics analyses. This work is supported by Alexander von Humboldt Foundation, the Helmholtz Alliance ICEMED, the Initiative and Networking Fund of the Helmholtz Association, the Helmholtz Initiative on Personalized Medicine iMed, the Helmholtz cross-program “Metabolic Dysfunction,” the Alfred Benzon Foundation, the Lundbeck Foundation, the German Research Foundation (TS226/3-1, Tu220/13-1, INST 40/492-1, SFB 1149, SFB 1123, SFB 1052, and ANR- 15-CE14-0030 [Nutripathos]), the European Research Council (ERC AdG°249929 and AdG° 695054), the German Center for Diabetes Research (DZD e.V.), and the German Federal Ministry of Education and Research (Infrafrontier grant 01KX1012).

Received: September 17, 2016

Revised: April 12, 2017

Accepted: August 28, 2017

Published: September 21, 2017

REFERENCES

- Anders, S., Pyl, P.T., and Huber, W. (2015). HTSeq—a Python framework to work with high-throughput sequencing data. *Bioinformatics* *31*, 166–169.
- Asensio, C., Muzzin, P., and Rohner-Jeanrenaud, F. (2004). Role of glucocorticoids in the physiopathology of excessive fat deposition and insulin resistance. *Int. J. Obes. Relat. Metab. Disord.* *28 (Suppl 4)*, S45–S52.
- Bullock, B.P., Heller, R.S., and Habener, J.F. (1996). Tissue distribution of messenger ribonucleic acid encoding the rat glucagon-like peptide-1 receptor. *Endocrinology* *137*, 2968–2978.
- Cavadas, C., Aveleira, C.A., Souza, G.F.P., and Velloso, L.A. (2016). The pathophysiology of defective proteostasis in the hypothalamus - from obesity to ageing. *Nat. Rev. Endocrinol.* *12*, 723–733.
- Cho, Y.M., Fujita, Y., and Kieffer, T.J. (2014). Glucagon-like peptide-1: glucose homeostasis and beyond. *Annu. Rev. Physiol.* *76*, 535–559.
- Cork, S.C., Richards, J.E., Holt, M.K., Gribble, F.M., Reimann, F., and Trapp, S. (2015). Distribution and characterisation of Glucagon-like peptide-1 receptor expressing cells in the mouse brain. *Mol. Metab.* *4*, 718–731.
- Coutinho, A.E., and Chapman, K.E. (2011). The anti-inflammatory and immunosuppressive effects of glucocorticoids, recent developments and mechanistic insights. *Mol. Cell. Endocrinol.* *335*, 2–13.
- Day, J.W., Ottaway, N., Patterson, J.T., Gelfanov, V., Smiley, D., Gidda, J., Findeisen, H., Bruemmer, D., Drucker, D.J., Chaudhary, N., et al. (2009). A new glucagon and GLP-1 co-agonist eliminates obesity in rodents. *Nat. Chem. Biol.* *5*, 749–757.
- Donath, M.Y. (2014). Targeting inflammation in the treatment of type 2 diabetes: time to start. *Nat. Rev. Drug Discov.* *13*, 465–476.
- Donath, M.Y., Dalmás, É., Sauter, N.S., and Böni-Schnetzler, M. (2013). Inflammation in obesity and diabetes: islet dysfunction and therapeutic opportunity. *Cell Metab.* *17*, 860–872.
- Douglass, J.D., Dorfman, M.D., Fasnacht, R., Shaffer, L.D., and Thaler, J.P. (2017). Astrocyte IKK β /NF- κ B signaling is required for diet-induced obesity and hypothalamic inflammation. *Mol. Metab.* *6*, 366–373.
- Dufour, J.H., Dziejman, M., Liu, M.T., Leung, J.H., Lane, T.E., and Luster, A.D. (2002). IFN- γ -inducible protein 10 (IP-10; CXCL10)-deficient mice reveal a role for IP-10 in effector T cell generation and trafficking. *J. Immunol.* *168*, 3195–3204.
- Finan, B., Yang, B., Ottaway, N., Stemmer, K., Müller, T.D., Yi, C.-X., Habegger, K., Schriever, S.C., García-Cáceres, C., Kabra, D.G., et al. (2012). Targeted estrogen delivery reverses the metabolic syndrome. *Nat. Med.* *18*, 1847–1856.
- Finan, B., Clemmensen, C., Zhu, Z., Stemmer, K., Gauthier, K., Müller, L., De Angelis, M., Moreth, K., Neff, F., Perez-Tilve, D., et al. (2016). Chemical hybridization of glucagon and thyroid hormone optimizes therapeutic impact for metabolic disease. *Cell* *167*, 843–857.e14.
- García-Cáceres, C., Quarta, C., Varela, L., Gao, Y., Gruber, T., Legutko, B., Jastroch, M., Johansson, P., Ninkovic, J., Yi, C.-X., et al. (2016). Astrocytic

- insulin signaling couples brain glucose uptake with nutrient availability. *Cell* 166, 867–880.
- Geer, E.B., Islam, J., and Buettner, C. (2014). Mechanisms of glucocorticoid-induced insulin resistance: focus on adipose tissue function and lipid metabolism. *Endocrinol. Metab. Clin. North Am.* 43, 75–102.
- Hadjijanni, I., Siminovitch, K.A., Danska, J.S., and Drucker, D.J. (2010). Glucagon-like peptide-1 receptor signalling selectively regulates murine lymphocyte proliferation and maintenance of peripheral regulatory T cells. *Diabetologia* 53, 730–740.
- Harder, H., Nielsen, L., Tu, D.T.T., and Astrup, A. (2004). The effect of liraglutide, a long-acting glucagon-like peptide 1 derivative, on glycemic control, body composition, and 24-h energy expenditure in patients with type 2 diabetes. *Diabetes Care* 27, 1915–1921.
- Heneka, M.T., Kummer, M.P., Stutz, A., Delekate, A., Schwartz, S., Vieira-Saecker, A., Griep, A., Axt, D., Remus, A., Tzeng, T.-C., et al. (2013). NLRP3 is activated in Alzheimer's disease and contributes to pathology in APP/PS1 mice. *Nature* 493, 674–678.
- Horvath, T.L., Sarman, B., García-Cáceres, C., Enriori, P.J., Sotonyi, P., Shanabrough, M., Borok, E., Argente, J., Chowen, J.A., Perez-Tilve, D., et al. (2010). Synaptic input organization of the melanocortin system predicts diet-induced hypothalamic reactive gliosis and obesity. *Proc. Natl. Acad. Sci. USA* 107, 14875–14880.
- Hotamisligil, G.S. (2017). Inflammation, metaflammation and immunometabolic disorders. *Nature* 542, 177–185.
- Ignacio-Souza, L.M., Bombassaro, B., Pascoal, L.B., Portovedo, M.A., Razolli, D.S., Coope, A., Victorio, S.C., de Moura, R.F., Nascimento, L.F., Arruda, A.P., et al. (2014). Defective regulation of the ubiquitin/proteasome system in the hypothalamus of obese male mice. *Endocrinology* 155, 2831–2844.
- Jais, A., and Brüning, J.C. (2017). Hypothalamic inflammation in obesity and metabolic disease. *J. Clin. Invest.* 127, 24–32.
- Jeanneteau, F.D., Lambert, W.M., Ismaili, N., Bath, K.G., Lee, F.S., Garabedian, M.J., and Chao, M.V. (2012). BDNF and glucocorticoids regulate corticotrophin-releasing hormone (CRH) homeostasis in the hypothalamus. *Proc. Natl. Acad. Sci. USA* 109, 1305–1310.
- Kälin, S., Heppner, F.L., Bechmann, I., Prinz, M., Tschöp, M.H., and Yi, C.-X. (2015). Hypothalamic innate immune reaction in obesity. *Nat. Rev. Endocrinol.* 11, 339–351.
- Kim, D., Kim, J., Yoon, J.H., Ghim, J., Yea, K., Song, P., Park, S., Lee, A., Hong, C.-P., Jang, M.S., et al. (2014a). CXCL12 secreted from adipose tissue recruits macrophages and induces insulin resistance in mice. *Diabetologia* 57, 1456–1465.
- Kim, J.G., Suyama, S., Koch, M., Jin, S., Argente-Arizon, P., Argente, J., Liu, Z.-W., Zimmer, M.R., Jeong, J.K., Szigeti-Buck, K., et al. (2014b). Leptin signaling in astrocytes regulates hypothalamic neuronal circuits and feeding. *Nat. Neurosci.* 17, 908–910.
- Kralisch, S., Bluher, M., Tonjes, A., Lossner, U., Paschke, R., Stumvoll, M., and Fasshauer, M. (2007). Tissue inhibitor of metalloproteinase-1 predicts adiposity in humans. *Eur. J. Endocrinol.* 156, 257–261.
- Kurz, T., Terman, A., Gustafsson, B., and Brunk, U.T. (2008). Lysosomes and oxidative stress in aging and apoptosis. *Biochim. Biophys. Acta* 1780, 1291–1303.
- Love, M.I., Huber, W., and Anders, S. (2014). Moderated estimation of fold change and dispersion for RNA-seq data with DESeq2. *Genome Biol.* 15, 550.
- Lumeng, C.N., and Saltiel, A.R. (2011). Inflammatory links between obesity and metabolic disease. *J. Clin. Invest.* 121, 2111–2117.
- Lynch, L., Hogan, A.E., Duquette, D., Lester, C., Banks, A., LeClair, K., Cohen, D.E., Ghosh, A., Lu, B., Corrigan, M., et al. (2016). iNKT cells induce FGF21 for thermogenesis and are required for maximal weight loss in GLP1 therapy. *Cell Metab.* 24, 510–519.
- Marco-Sola, S., Sammeth, M., Guigó, R., and Ribeca, P. (2012). The GEM mapper: fast, accurate and versatile alignment by filtration. *Nat. Methods* 9, 1185–1188.
- Marx, N., Burgmaier, M., Heinz, P., Ostertag, M., Hausauer, A., Bach, H., Durst, R., Hombach, V., and Walcher, D. (2010). Glucagon-like peptide-1 (1–37) inhibits chemokine-induced migration of human CD4-positive lymphocytes. *Cell. Mol. Life Sci.* 67, 3549–3555.
- Meagher, C., Beilke, J., Arreaza, G., Mi, Q.-S., Chen, W., Salojin, K., Horst, N., Cruikshank, W.W., and Delovitch, T.L. (2010). Neutralization of interleukin-16 protects nonobese diabetic mice from autoimmune type 1 diabetes by a CCL4-dependent mechanism. *Diabetes* 59, 2862–2871.
- Meissburger, B., Stachorski, L., Röder, E., Rudofsky, G., and Wolfrum, C. (2011). Tissue inhibitor of matrix metalloproteinase 1 (TIMP1) controls adipogenesis in obesity in mice and in humans. *Diabetologia* 54, 1468–1479.
- Milanski, M., Degasperi, G., Coope, A., Morari, J., Denis, R., Cintra, D.E., Tsukumo, D.M.L., Anhe, G., Amaral, M.E., Takahashi, H.K., et al. (2009). Saturated fatty acids produce an inflammatory response predominantly through the activation of TLR4 signaling in hypothalamus: implications for the pathogenesis of obesity. *J. Neurosci.* 29, 359–370.
- Miller, A.H., Spencer, R.L., Pulera, M., Kang, S., McEwen, B.S., and Stein, M. (1992). Adrenal steroid receptor activation in rat brain and pituitary following dexamethasone: implications for the dexamethasone suppression test. *Biol. Psychiatry* 32, 850–869.
- Osaka, M., Ito, S., Honda, M., Inomata, Y., Egashira, K., and Yoshida, M. (2016). Critical role of the C5a-activated neutrophils in high-fat diet-induced vascular inflammation. *Sci. Rep.* 6, 21391.
- Ozcan, L., Ergin, A.S., Lu, A., Chung, J., Sarkar, S., Nie, D., Myers, M.G., Jr., and Ozcan, U. (2009). Endoplasmic reticulum stress plays a central role in development of leptin resistance. *Cell Metab.* 9, 35–51.
- Patel, R., Williams-Dautovich, J., and Cummins, C.L. (2014). Minireview: new molecular mediators of glucocorticoid receptor activity in metabolic tissues. *Mol. Endocrinol.* 28, 999–1011.
- Quarta, C., Sánchez-Garrido, M.A., Tschöp, M.H., and Clemmensen, C. (2016). Renaissance of leptin for obesity therapy. *Diabetologia* 59, 920–927.
- Schäcke, H., Döcke, W.D., and Asadullah, K. (2002). Mechanisms involved in the side effects of glucocorticoids. *Pharmacol. Ther.* 96, 23–43.
- Scrocchi, L.A., Brown, T.J., McClusky, N., Brubaker, P.L., Auerbach, A.B., Joyner, A.L., and Drucker, D.J. (1996). Glucose intolerance but normal satiety in mice with a null mutation in the glucagon-like peptide 1 receptor gene. *Nat. Med.* 2, 1254–1258.
- Secher, A., Jelsing, J., Baquero, A.F., Hecksher-Sørensen, J., Cowley, M.A., Dalbøge, L.S., Hansen, G., Grove, K.L., Pyke, C., Raun, K., et al. (2014). The arcuate nucleus mediates GLP-1 receptor agonist liraglutide-dependent weight loss. *J. Clin. Invest.* 124, 4473–4488.
- Shai, I., Pischon, T., Hu, F.B., Ascherio, A., Rifai, N., and Rimm, E.B. (2006). Soluble intercellular adhesion molecules, soluble vascular cell adhesion molecules, and risk of coronary heart disease. *Obesity (Silver Spring)* 14, 2099–2106.
- Shoelson, S.E., Lee, J., and Goldfine, A.B. (2006). Inflammation and insulin resistance. *J. Clin. Invest.* 116, 1793–1801.
- Sisley, S., Gutierrez-Aguilar, R., Scott, M., D'Alessio, D.A., Sandoval, D.A., and Seeley, R.J. (2014). Neuronal GLP1R mediates liraglutide's anorectic but not glucose-lowering effect. *J. Clin. Invest.* 124, 2456–2463.
- Smith, E.P., An, Z., Wagner, C., Lewis, A.G., Cohen, E.B., Li, B., Mahbod, P., Sandoval, D., Perez-Tilve, D., Tamarina, N., et al. (2014). The role of β cell glucagon-like peptide-1 signaling in glucose regulation and response to diabetes drugs. *Cell Metab.* 19, 1050–1057.
- Thaler, J.P., Yi, C.-X., Schur, E.A., Guyenet, S.J., Hwang, B.H., Dietrich, M.O., Zhao, X., Sarruf, D.A., Izgur, V., Maravilla, K.R., et al. (2012). Obesity is associated with hypothalamic injury in rodents and humans. *J. Clin. Invest.* 122, 153–162.
- Tschöp, M.H., Speakman, J.R., Arch, J.R.S., Auwerx, J., Brüning, J.C., Chan, L., Eckel, R.H., Farese, R.V., Jr., Galgani, J.E., Hambly, C., et al. (2011). A guide to analysis of mouse energy metabolism. *Nat. Methods* 9, 57–63.
- Tschöp, M.H., Finan, B., Clemmensen, C., Gelfanov, V., Perez-Tilve, D., Müller, T.D., and DiMarchi, R.D. (2016). Unimolecular polypharmacy for treatment of diabetes and obesity. *Cell Metab.* 24, 51–62.

Valdearcos, M., Robblee, M.M., Benjamin, D.I., Nomura, D.K., Xu, A.W., and Koliwad, S.K. (2014). Microglia dictate the impact of saturated fat consumption on hypothalamic inflammation and neuronal function. *Cell Rep.* **9**, 2124–2138.

Valdearcos, M., Xu, A.W., and Koliwad, S.K. (2015). Hypothalamic inflammation in the control of metabolic function. *Annu. Rev. Physiol.* **77**, 131–160.

Vandanmagsar, B., Youm, Y.-H., Ravussin, A., Galgani, J.E., Stadler, K., Mynatt, R.L., Ravussin, E., Stephens, J.M., and Dixit, V.D. (2011). The NLRP3 inflammasome instigates obesity-induced inflammation and insulin resistance. *Nat. Med.* **17**, 179–188.

Weisberg, S.P., McCann, D., Desai, M., Rosenbaum, M., Leibel, R.L., and Ferrante, A.W., Jr. (2003). Obesity is associated with macrophage accumulation in adipose tissue. *J. Clin. Invest.* **112**, 1796–1808.

Wilson-Pérez, H.E., Chambers, A.P., Ryan, K.K., Li, B., Sandoval, D.A., Stoffers, D., Drucker, D.J., Pérez-Tilve, D., and Seeley, R.J. (2013). Vertical sleeve gastrectomy is effective in two genetic mouse models of glucagon-like Peptide 1 receptor deficiency. *Diabetes* **62**, 2380–2385.

Yi, C.-X., Walter, M., Gao, Y., Pitra, S., Legutko, B., Kälén, S., Layritz, C., García-Cáceres, C., Bielohuby, M., Bidlingmaier, M., et al. (2017). TNF α drives mitochondrial stress in POMC neurons in obesity. *Nat. Commun.* **8**, 15143.

Zhang, F., Basinski, M.B., Beals, J.M., Briggs, S.L., Churgay, L.M., Clawson, D.K., DiMarchi, R.D., Furman, T.C., Hale, J.E., Hsiung, H.M., et al. (1997). Crystal structure of the obese protein leptin-E100. *Nature* **387**, 206–209.

Zhang, X., Zhang, G., Zhang, H., Karin, M., Bai, H., and Cai, D. (2008). Hypothalamic IKK β /NF- κ B and ER stress link overnutrition to energy imbalance and obesity. *Cell* **135**, 61–73.

STAR★METHODS

KEY RESOURCES TABLE

REAGENT or RESOURCE	SOURCE	IDENTIFIER
Antibodies		
Rabbit polyclonal anti-iba1	Synaptic Systems	Cat. No. 234 003; RRID: AB_10641962
Rabbit polyclonal anti-GFAP	DAKO	Cat. No. Z0334; RRID: AB_10013382
Biotinylated Goat anti-Rabbit IgG A	Vector	Cat. No. BA-1000; RRID: AB_2313606
POMC precursor (27-52) (Porcine)	Phoenix Pharmaceuticals	Cat. No. H-029-30; RRID: AB_2307442
Rabbit anti-Insulin (C27C9)	Cell Signaling	Cat. No. 3014; RRID: AB_2126503
Guinea pig anti-Glucagon	TAKARA	Cat. No. M182; RRID: AB_2619627
Goat anti-Somatostatin (D-20)	Santa Cruz	Cat. No. sc-7819; RRID: AB_2302603
Chemicals, Peptides, and Recombinant Proteins		
GLP-1	This paper	N/A
GLP-1/Dexa	This paper	N/A
GLP-1/Dexa (H-C-D)	This paper	N/A
GLP-1/Dexa (C-D)	This paper	N/A
Dexamethasone	Sigma-Aldrich	Cat. No. D1756
3,3'-Diaminobenzidine tetrahydrochloride hydrate	Sigma-Aldrich	Cat. No. 32750
AraC (cytosine-1-β-D-arabinofuranoside)	Sigma-Aldrich	Cat. No. C1768
Tamoxifen, Free base	Sigma-Aldrich	Cat. No. T5648
Paraformaldehyde (PFA)	Serva	Cat. No. 31628-02
Uranyl acetate	Serva	Cat. No. 77870
Glutaraldehyde	Serva	Cat. No. 23114.01
Propylene oxide	Sigma Aldrich	Cat. No. 82320
Durcupan	Sigma Aldrich	Cat. No. 44610-1EA
Osmium tetroxide	EMS	Cat. No. 19170
Formvar solution	Science Services	Cat. No. E15830-25
Lead citrate	Science Services	Cat. No. E22410
Human Leptin E100	Zhang et al., 1997	N/A
Buprenorphine, Buprécare	Axience (Pantin, France)	Cat. No. 03760087151244
Meloxicam, Metacam	Boehringer Ingelheim (Reims, France)	Cat. No. 04028691523598
Lidocaine, lurocaine 2%	Vétoquinol (Paris, France)	Cat. No. 03605877020815
Critical Commercial Assays		
Vectastain ABC HRP Kit (Peroxidase, Standard)	Vector	Cat. No. PK-4000
Vectastain Elite ABC HRP Kit	Vector	Cat. No. PK-6100
C-terminal collagen crosslinks (CTX-1) EIA kit	ELISA Immuno Diagnostic Systems	Cat. No. AC-06F1
N-terminal propeptide of type 1 collagen (PINP) EIA kit	ELISA Immuno Diagnostic Systems	Cat. No. AC-33F1
Corticosterone EIA Kit	Arbor Assays	Cat. No. K014-H1
Mouse Insulin ELISA kit	Crystal Chem	Cat. No. 90082
Proteome Profiler Mouse Cytokine Array kit Panel A	R&D systems	Cat. No. ARY006
mTNF HTRF Assay Kit	CisBio	Cat. No. 6FMTNPEH
mIL1b HTRF Assay Kit	CisBio	Cat. No. 63ADk010pec
mIL6 HTRF Assay Kit	CisBio	Cat. No. 63ADK043PEB
Deposited Data		
RNA sequencing data	GEO	GEO: GSE102415
Experimental Models: Cell Lines		
Human: HEK293 cells	ATCC	Cat. No. CRL-1573

(Continued on next page)

Continued

REAGENT or RESOURCE	SOURCE	IDENTIFIER
Experimental Models: Organisms/Strains		
Mouse: DIO: C57bl6j	Jackson Laboratories	JAX: 000664
Mouse: Glp1r ^{-/-}	Scrocchi et. al. 1996	N/A
Mouse: Glp1r ^{flox/flox}	Wilson-Pérez et al., 2013	N/A
Mouse: nestin-Cre	Jackson Laboratories	JAX: 003771
Mouse: nestin-Cre Glp1r ^{flox/flox}	Sisley et al., 2014	N/A
Mouse: MIP-ER-Cre	Jackson Laboratories	JAX: 024709
Mouse: MIP-creER Glp1r ^{flox/flox}	Smith et al., 2014	N/A
Mouse: <i>ob/ob</i>	Jackson Laboratories	JAX: 000632
Oligonucleotides		
qPCR primers	See Table S1	N/A
Recombinant DNA		
Human GLP-1R cDNA	Finan et. al. 2012	N/A
Luciferase reporter construct	Finan et. al. 2012	N/A
Software and Algorithms		
GraphPad prism 6.0b	GraphPad	N/A
Other		
Indirect calorimetry system - TSE PhenoMaster	TSE Systems, Germany	N/A
High fat/high sugar diet	Research Diets	Cat. No. D12331
High fat diet	Research Diets	Cat. No. D12492

CONTACT FOR REAGENT AND RESOURCE SHARING

Further information and requests for reagents may be directed to and will be fulfilled by the Lead Contact, Brian Finan (brian.finan@helmholtz-muenchen.de).

EXPERIMENTAL MODEL AND SUBJECT DETAILS**Mice**

All animal experiments were approved and conducted under the guidelines of the Institutional Animal Care and Use Committees of the Helmholtz Center Munich and the University of Cincinnati. For the DIO studies, male C57bl6j mice (Jackson Laboratories) were fed a diabetogenic diet (D12331; Research Diets, New Brunswick, NJ. 58% kcal from fat, 25.5% kcal from carbohydrates, and 16.4% kcal from protein) beginning at 8 weeks of age. Mice were maintained under these conditions for a minimum of 16 weeks before initiation of pharmacological studies, and were between the ages of 6 months and 8 months old. Mice were randomized and evenly distributed among test groups according to body weight and body composition. Mice were double housed with a 12-h/12-h light-dark cycle at 22°C and free access to food and water.

Male Glp1r^{-/-} mice (herein named global KO mice) and wild-type mice were generated as previously described. Male neuronal GLP-1R conditional knockout mice (nestin-Cre Glp1r^{flox/flox}) and wild-type littermates were generated as previously described ([Sisley et al., 2014](#)) and fed a diabetogenic diet containing 60% kcal from fat (D12492; Research Diets, New Brunswick, NJ). Male mice with the selective ablation of GLP-1Rs in pancreatic β -cells were generated by crossing GLP-1R f/f mice with mice expressing CRE recombinase in the β -cells under tamoxifen-inducible regulation using a mouse insulin promoter (MIP-creERT Glp1r^{flox/flox} mice, herein named β -cell-KO), as previously described ([Smith et al., 2014](#)). Glp1r^{f/f} male littermates were used as control animals. Tamoxifen (1mg/kg i.p., free base, Sigma-Aldrich #T5648) was administered to β -cell-KO mice and to control animals as previously described ([Smith et al., 2014](#)), in mice fed with a diabetogenic diet containing 60% kcal from fat (D12492; Research Diets, New Brunswick, NJ). The studies in *ob/ob* mice were performed using 9-week-old male mice (The Jackson Laboratory, stock no. 000632) fed with chow diet. All the compounds used in the study were injected subcutaneously at equimolar doses of 100 nmol/kg unless otherwise mentioned. Compounds were administered in a vehicle solution containing PBS unless otherwise mentioned. Compounds were given by daily subcutaneous (s.c.) injections at the indicated doses at a volume of 5 μ L per g of body weight unless otherwise mentioned.

METHOD DETAILS

Peptide Synthesis and Validation

As the peptide vector, we utilized a GLP-1 analog previously shown to retain full potency at GLP-1 receptor and protected from DPP-IV-mediated degradation (Finan et al., 2012). The GLP-1 peptide backbones feature the three different C-terminal, thiol-containing amino acids were constructed by standard Fmoc-based solid phase peptide synthesis on a rink amide ChemMatrix resin, cleaved from the solid support by TFA, and subsequently purified by reversed-phase HPLC. To derivatize DEXA with the bioactivatable linker and free thiol to facilitate coupling to the peptide, native DEXA (Sigma-Aldrich) was first reacted with 4-nitrophenyl chloroformate in pyridine to yield dexamethasone-nitrophenyl ester. In a single pot synthesis, the DEXA nitrophenyl ester was further reacted with pyridyl-dithioethylamine in the presence of DIEA. The resulting activated derivative of DEXA was mixed with the unique, thiol-containing GLP-1 analogs in a urea-containing phosphate buffer (pH~7.0) to afford the various GLP-1-DEXA conjugates. The conjugates obtained after preparative reverse-phase HPLC purification were confirmed by electrospray mass spectrometry. GLP-1/DEXA and GLP-1 were individually tested for their ability to activate the GLP-1 receptor through a cell-based luciferase reporter gene assay that indirectly measures cAMP induction. Human embryonic kidney (HEK293) cells were co-transfected with human GLP-1R receptor cDNA (zeocin-selection) and a luciferase reporter gene construct fused to a cAMP response element (CRE) (hygromycin B-selection), as in Finan et al. (2012). Cells were seeded at a density of 22,000 cells per well and serum deprived for 16 hr in DMEM (HyClone) supplemented with 0.25% (vol/vol) bovine growth serum (BGS) (HyClone). Serial dilutions of the peptides were added to 96-well cell-culture treated plates (BD Biosciences) containing the serum-deprived, co-transfected HEK293 cells, and incubated for 5 hr at 37°C and 5% CO₂ in a humidified environment. To stop the incubation, an equivalent volume of Steady Lite HTS luminescence substrate reagent (Perkin Elmer) was added to the cells to induce lysis and expose the lysates to luciferin. The cells were agitated for 5 min and stored for 10 min in the dark. Luminescence was measured on a MicroBeta-1450 liquid scintillation counter (Perkin-Elmer). Luminescence data were graphed against peptide concentrations and EC₅₀ values were calculated using Origin software (OriginLab).

Body Composition Measurements

Body composition (fat and lean mass) was measured using quantitative nuclear magnetic resonance technology (EchoMRI, Houston, TX).

Dual-Energy X-Ray Absorptiometry (DEXA)

Body and spine BMD were determined by scanning decapitated/eviscerated carcasses (fixed in 70% ethanol) using an UltraFocusDXA (Faxitron Bioptics, Tucson, AZ USA) with pixel dimensions of 48 μm. After body BMD was measured the Region of Interest (ROI) function was employed to determine BMD of spine LV2 through LV5. Bone areas, BMC and vBMD (BMD divided by the square root of bone area) were also determined.

Glucose Metabolism Assessments

For the analysis of glucose tolerance, mice were intraperitoneally injected with 1.5 g glucose per kg of BW [20% (wt/v) D glucose (Sigma-Aldrich) in 0.9% (wt/v) saline], unless otherwise mentioned. Tail blood glucose concentrations (mg/dl) were measured using a handheld glucometer (TheraSense Freestyle). For insulin release, mice were fasted for 6 hr and intraperitoneally injected with 1.5 g glucose per kg of BW [20% (wt/v) D glucose (Sigma-Aldrich) in 0.9% (wt/v) saline]. Plasma levels of insulin were measured using a commercially available kit (Crystal Chem # 90082) according to the manufacturer's instructions.

For the determination of insulin sensitivity, mice were fasted for 6h and intraperitoneally injected with 0.7 U of insulin per kg of BW (0.1 U/ml; Humalog Pen, Eli Lilly). Tail blood glucose concentrations were measured using a handheld glucometer (TheraSense FreeStyle) before (0 min) and at 15, 30, 60, and 120 min after injection.

Leptin Challenge

DIO mice (N = 16) received the compounds via a single s.c. injection 7 hr prior the onset of the dark phase, which was 6 hr before the leptin bolus. During those 6 hr, food was withdrawn. Mice receiving each treatment were sub-divided (N = 8) to receive a bolus of saline or leptin. Saline or leptin (3 or 5 mg/kg; i.p.) were injected 1 hr before the dark phase and food was provided immediately following the injection. Food intake was measured at the indicated time points over the next 24 hr. Following that acute leptin challenge, these DIO mice were treated for 6 days via daily s.c. injections of vehicle, DEXA, GLP-1, or two doses of GLP-1/DEXA (N = 16). 24 hr following the last injection of the compounds on day 7, an acute leptin challenge test was performed again using the same sub-group stratification (N = 8), fasting period (6h), dose of leptin (3 mg/kg; i.p.), and food intake sampling. Animals were treated with Human Leptin E100 (Zhang et al., 1997).

Indirect Calorimetry

Energy expenditure and respiratory exchange ratio were assessed using a combined indirect calorimetry system (TSE PhenoMaster, TSE Systems, Bad Homburg, Germany). O₂ consumption and CO₂ production were measured every 10 min for a total of up to 120 hr (after 48 hr of adaptation). Energy expenditure (EE, kcal/h) values were correlated to the body weight of the animals recorded at the end of the measurement using ANCOVA analysis of variance, as shown in Tschöp et al. (2011).

Intracerebroventricular (i.c.v.) Studies

20-week-old male mice (C57Bl6j) were pre-treated with buprenorphine (0.18 mg/kg) and lidocaine (6 mg/kg) before surgery, anesthetized with isoflurane (induction: 3%; 2L/min, mask: 2%; 0.2 L/min and progressively reduced to obtained 0.8% at the end of surgery), and then implanted with a cannula (Alzet brain infusion kit 3, Charles River, France) into the lateral ventricle (anteroposterior: –0.5 mm from bregma, lateral: $-/+1; \pm 2$ mm to bregma and dorsoventral: –2.1 mm below skull) using a stereotaxic apparatus (David Kopf Instruments, USA). The cannula was connected to an Alzet osmotic minipump (flow rate of 0.19 μ l/h for fourteen days, Alzet model 1002, Charles River, France) via a 36.6 mm-long vinyl tubing (inner diameter 0.69 mm) filled with 0.9% saline (Coopération pharmaceutique Française, France). The minipumps were filled with 0.9% saline, GLP-1, Dexa, or GLP-1/Dexa (all drugs at 0.1 μ g/24h; 0.0219 μ g/ μ l each), then primed overnight at 37°C in 0.9% saline before subcutaneous implantation. At the end of surgery mice received subcutaneously meloxicam (3 mg/kg in 0.3ml saline) as post-surgical anti-pain medication. Meloxicam injections were repeated once the next day.

Gene Expression Analysis by qPCR

For tissue collection, mice were fasted for 4 hr and treated with compounds 2 hr prior to tissue collection. Dissected tissues were immediately frozen on dry ice, and RNA was extracted using RNeasy Mini Kits (QIAGEN). Quantitative Real-Time RT-PCR (qPCR) was performed with a ViiA 7 Real-Time PCR System (Applied Biosystems) using either TaqMan probes (Applied Biosystems, Carlsbad, CA, USA) or custom-made primers (Sigma-Aldrich, St Louis, MO, USA). Target gene expression was normalized to reference genes *Hprt* or *Ppib* and calculated relative to saline vehicle-treated controls. Primers sequences are indicated in [Table S1](#).

Corticosterone Measurement

Blood was collected from tail veins at 8 AM or 5 PM, immediately chilled on ice, centrifuged at 5,000 g at 4°C. Plasma corticosterone was quantified by DetectX immunoassay kit (Arbor Assays, #K014-H1) according to the manufacturers' instructions.

Markers of Bone Metabolism

Plasma levels of C-terminal collagen crosslinks (CTX) and N-terminal propeptide of type 1 collagen (P1NP) were measured using ELISA assays (ELISA Immuno Diagnostic Systems, #AC-06F1 and #AC-33F1) according to the manufacturers' instructions.

Immunohistochemistry

Mice were transcardially perfused with phosphate-buffered saline (PBS) followed by 4% neutral buffered paraformaldehyde (Fisher Scientific). After dissection, brains were equilibrated in 30% sucrose, sectioned coronally on a cryostat (Leica Biosystems) at 30 μ m and collected and rinsed in 0.1 M TBS. Brain sections were incubated with a primary antibody anti-iba1 (made in rabbit, 1:1500, Synaptic Systems, Germany), or anti-GFAP (made in rabbit, 1:2000, DAKO, Germany). Primary antibodies were incubated overnight at 4°C and sections were rinsed and incubated with biotinylated secondary goat anti-rabbit IgG, followed by incubation in avidin-biotin complex (ABC method, Vector Laboratories, Burlingame, CA) for 1 hr. The reaction product was visualized by incubation in 1% diaminobenzidine with 0.01% hydrogen peroxide for 5-7 min. Sections were mounted on gelatin-coated glass slides, dried, dehydrated through a graded ethanol series, cleared in xylene, and coverslipped for image quantification. A Zeiss AXIO Scope A1 microscope was used for image analysis. Image quantification was blinded; cell numbers were manually counted within a frame outlining 0.06mm² inside the ARC using ImageJ. Immunohistochemistry in pancreatic tissues was performed using cryosections (20 μ m) stained with the following antibodies: rabbit anti-insulin (1.3000, Cell signaling, #3014), guinea pig anti-glucagon (1.2500, TAKARA, #M182), goat anti-somatostatin (1.300, Santa Cruz, #sc-7819). Images of pancreatic islets were obtained with a Leica microscope (DMI 6000) using the LAS AF software. The Images were analyzed using LAS AF software. For quantification, the mean signal intensity per islet area was measured.

Adipose Tissue Histology

Visceral and subcutaneous fat pads were fixed and stored in 4% paraformaldehyde after dissection. After dehydration, tissues were embedded in paraffin using Leica embedding machine (EG1150 H) and cut in 5 μ m sections using Leica Microtome (RM2255) to perform H&E staining. Samples were stained with hematoxylin for 2:45 min and eosinY for 1:30 min and fixed with Roti-Histokitt (Carl Roth) before analyzing them independently using Microscope Scope A.1 (Zeiss). The numbers of crown-like structures within 8 regions of interest were quantified by two independent observers in 3 different adipose samples per group.

Electron Microscopy

Animals were sacrificed and transcardially perfused using 4% paraformaldehyde solution (Serva, Heidelberg, Germany) containing 0.1% glutaraldehyde (Serva) in phosphate-buffered saline, and fixed for 10 hr. Serial hypothalamic sections (50 μ m) were collected in Tris (Sigma-Aldrich, Steinheim, Germany)-buffered saline (TBS) and treated with different alcohol concentrations: 10%, 20%, 30%, 40% and 50% for 5 min, each, to unhinge lipids for permeabilization. Next, sections were rinsed in TBS for 5 min and incubated in 5% normal goat serum (NGS) in TBS for 30min at RT, followed by overnight incubation with POMC primary antibody at RT (dilution 1:1,000 in TBS containing 1% NGS; POMC precursor (27-52) (Porcine), H-029-30; Phoenix Pharmaceuticals, Burlingame, CA, USA). The next day, a 6x 5min wash steps using TBS were performed and the biotin-conjugated goat anti-rabbit IgG secondary antibody (dilution 1:200 in 0.5% NGS in TBS; Vector Laboratories, Burlingame, CA, USA) was added to the sections for 2h at RT.

Afterward, sections were washed 6 times for 5 min in TBS, incubated with ABC complex (Vectastain Elite ABC HRP Kit, # PK-6100, Vector Laboratories) for 45min at RT and developed with 3,3-diaminobenzidine (DAB). After transfer in PBS and thorough rinsing, sections were stained with 0.5% osmium tetroxide (EMS, Hatfield, PA, USA) in PBS for 30 min, followed by dehydration in graded ethanol and additional staining with 1% uranyl acetate in 70% ethanol for 1h. After final dehydration in 100% ethanol and propylene oxide (Sigma-Aldrich) sections were incubated in Durcupan (Sigma-Aldrich) and embedded between coated microscope slides and cover glasses followed by polymerization for 48h at 56°C. Regions of interest were identified by light microscopy, trimmed, transferred onto blocks of resin and cut using an ultra-microtome (Leica Microsystems). Ultra-thin sections were transferred on formvar-coated grids and stained with lead citrate for 6 min. Electron Microscopy was performed using a Zeiss SIGMA electron microscope (Zeiss NTS, Oberkochen, Germany) equipped with a STEM detector. Semi-quantification was performed by analyzing and counting of lipofuscin granules in cross-sectioned POMC-immunopositive neurons, with an average number of 23 and no fewer than 16 neurons per animal ($n = 4$ per group) analyzed.

Hypothalamic Cytokine Measurement

Detection of cytokines in mouse hypothalamus lysates was performed by high-throughput homogeneous time-resolved fluorescence (HTRF) sandwich immunoassays (Cisbio Assays, France), using specific anti-TNF α , anti-IL-1 β , or anti-IL-6 labeled with Eu3+-Cryptate and second anti-TNF α , anti-IL-1 β , or anti-IL-6 labeled with d2. Samples were mixed with a solution containing antibodies targeting the respective cytokines conjugated with Eu3+ cryptate fluorescence resonance energy transfer (FRET) donor, and the d2 FRET acceptor (volume ratio of 4:1) in medium binding white bottom HTRFP compatible 384-well plates in 20 μ L assay total volume per well. Measurements were made using a Spectra Max i3x Multi-Mode Microplate Reader (Molecular Devices) by exciting the fluorescence donor at 337 nm and simultaneously reading fluorescence emission at 620 nm (donor emission) and 665 nm (acceptor emission). The HTRF signal was calculated as the E665/E620 ratio. Calibration curves were prepared using recombinant cytokines dissolved in buffers corresponding to the composition of the tested lysates. Reactions were allowed to incubate overnight. The E665/E620 ratio values of the calibration standards were fitted to a 4-parameter equation and cytokine concentrations in the experimental samples were calculated on the basis of these standard curve data.

Plasma Cytokine Measurement

Cytokine and chemokine levels in plasma were evaluated using a proteome profiler array kit (Mouse Cytokine Array Panel A, R&D Systems) according to the manufacturer's instructions. Plasma samples (300 μ L) were mixed with the biotinylated detection antibody cocktail at room temperature for one hour while the array membrane was blocked with the blocking buffer supplied by the manufacturer. The membranes were incubated with the samples overnight at 4°C. After washing, the membranes were incubated with HRP-conjugated Streptavidin for 30 min at room temperature. Signal was achieved using chemiluminescent detection reagents, detected with LI-COR Odyssey and was analyzed using Image Studio Lite software (LI-COR BioSciences).

Culture of Hypothalamic Primary Neurons

Hypothalami from E14 WT mice or Glp1r $^{-/-}$ mice were extracted in ice cold calcium and magnesium free HBSS (Life Technologies), digested for 10 min at 37°C with 0.05% trypsin (Life Technologies), washed three times with PBS and dispersed in serum free MEM supplemented with L-glutamine (2mM) and glucose (25mM). Cells were plated on 12-well plates coated with poly-L-lysine (Sigma-Aldrich) at 1.5 X10⁶ per well in MEM supplemented with heat-inactivated 10% horse serum, and 10% fetal bovine serum, 2mM L-glutamine and glucose (25mM) without antibiotics. On day 4, half the medium was exchanged with fresh culture medium lacking fetal bovine serum, and containing 10 μ M mitotic inhibitor AraC (cytosine-1- β -D-arabinofuranoside, #C1768 Sigma-Aldrich) to inhibit non-neuronal cell proliferation. Experiments were performed on neurons grown in culture for 7 days. Supplemented MEM was exchanged for MEM without any supplements and neurons were treated with vehicle or GLP-1/Dexa (200nM) for 6 hr before RNA extraction.

RNA Sequencing

Prior library preparation RNA integrity was determined with the Agilent 2100 Bioanalyzer using the RNA 6000 Nano Kit. All samples had a RNA integrity number (RIN) value greater than 7. For library preparation, 1 μ g of total RNA per sample was used. Library construction was performed as described in the Low Throughput protocol of the TruSeq RNA Sample Prep Guide (Illumina) in an automated manner using the Bravo Automated Liquid Handling Platform (Agilent). cDNA libraries were assessed for quality and quantity with the Lab Chip GX (Perkin Elmer) and the Quant-iT PicoGreen dsDNA Assay Kit (Life Technologies). RNA libraries were sequenced as 100 bp paired-end runs on an Illumina HiSeq4000 platform. On average, about 8 Gb of sequence per sample were obtained. The GEM mapper (Marco-Sola et al., 2012) (v 1.7.1) with modified parameter settings (mismatches = 0.04, min-decoded-strata = 2) was used for split-read alignment against the human genome assembly mm9 (NCBI37) and UCSC knownGene annotation. To quantify the number of reads mapping to annotated genes we used HTseq-count (Anders et al., 2015) (v0.6.0). FPKM (Fragments Per Kilobase of transcript per Million fragments mapped) values were calculated using custom scripts. Duplicate reads were removed. For comparison, the relative coverage was calculated separately for each sample by dividing the coverage at each position by the number of reads mapped to mtDNA multiplied by 1Mio (average number of mapped reads was 0.85 Mio over all samples). Gene expression values were estimated using Bioconductors R package DESeq2 (Love et al., 2014). Significant regulation was estimated using one-way ANOVA with false discovery correction using the Benjamini Hochberg procedure and a $p < 0.01$ cut-off. Significance of

KEGG enrichments was estimated using a hypergeometric distribution test. All calculations were performed using R and MATLAB (MATLAB and Statistics Toolbox Release 2015b, The MathWorks, Natick, Massachusetts, United States).

QUANTIFICATION AND STATISTICAL ANALYSIS

Statistical analyses were performed using Graph Prism 6 (GraphPad Software, San Diego, CA USA). Results are expressed as mean \pm SEM unless otherwise specified. Two groups were compared using unpaired two-tail Student's t test. For more than two groups, one- or two-way ANOVA was used, as appropriate, followed by Tukey post hoc adjustment. Repeated-measures ANOVA was also used whenever appropriate. Differences with P values less than 0.05 were considered significant.

DATA AND SOFTWARE AVAILABILITY

The accession number for the RNA sequencing data reported in this paper is GEO: GSE102415.